3-8-93
E-7237

NASA Technical Memorandum 105824

Structural Dynamics Branch Research and Accomplishments for FY 1992

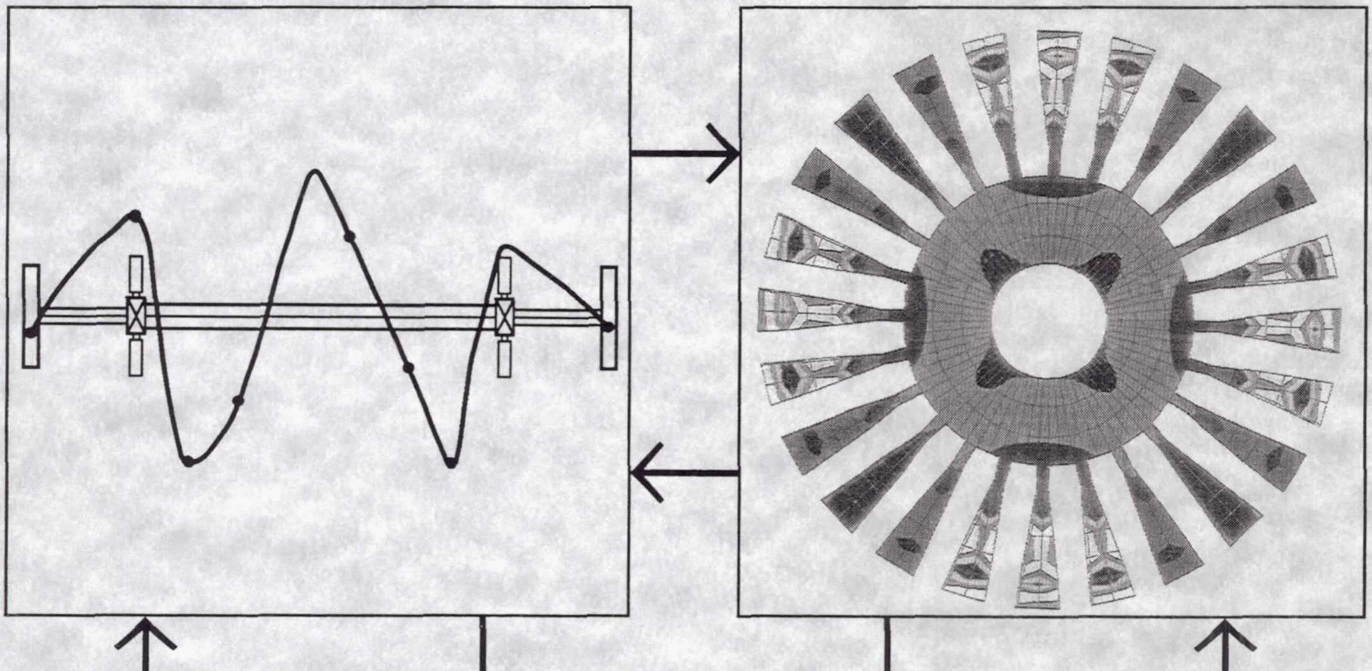

December 1992
Lewis Research Center

INTRODUCTION

INTRODUCTION

This document highlights some of the technical accomplishments of the Structural Dynamics Branch at NASA's Lewis Research Center for fiscal year 1992. We have included some of our more significant accomplishments of the past year.

The Structural Dynamics Branch conducts research in advanced propulsion and power systems as well as precision mechanical systems. Our work directly supports NASA's longer-term aeronautical and space system program goals. We support turboprop, space shuttle main engine, the national aerospace plane, space power, the numerical propulsion simulator and space mechanisms programs. We are also involved in a number of cooperative technology development programs with our industrial colleagues. This work can be broadly classified into four major activities: turbomachinery aeroelasticity, turbomachinery vibration control, dynamic systems response and analysis, and computational structural methods.

In aeroelasticity, we are developing improved analytical and experimental methods for avoiding flutter and minimizing forced vibration response of aerospace propulsion systems. Work elements include classical (frequency domain) methods, time domain methods, computational methods for fluid-coupled structural response, experimental methods, and application studies (turboprop, turbofan, turbopump, and advanced core technology). We have maintained an increased emphasis on the problems associated the forced vibration response of SSME class turbomachinery blading and prop-fan systems.

In vibration control we conceive, analyze, develop and demonstrate new methods to control vibrations an aerospace systems to increase life and performance. Work elements include actively controlled structures, passive vibration control methods, computational methods for active vibration control, and application studies (vibration isolation, magnetic and piezo-actively controlled bearings, and cryo turbo machinery). This area continues to be a major focus for us. We are emphasizing new control algorithms and approaches for extremely low power consuming magnetic bearings which can operate in thermal extremes (cryogenic at one end and 1000 degrees fahrenheit at the other) .

Dynamic systems work is directed to analyzing and verifying the dynamics of interacting systems principally in aerospace propulsion and space based power systems. Work elements include space mechanisms , computational methods for dynamics analysis and application studies (space lab mechanisms and robotics, NASP engine sealing concepts, and parallel computing for dynamics analysis). We have completed labs and are conducting experiments to develop extremely long life rolling element bearings for space service and establish requisite tools for designers.

Our work in computational methods is not considered a separate activity. Rather, computational methods development has been folded in with the objectives of the three other major focus areas within the branch. The goal of this work is to fundamentally improve the use of modern computers for the solution of realistic structural dynamics problems, with a particular emphasis on parallel processing. In aeroelasticity, computational methods work is focused on time-domain solutions and coupled fluid structure interaction. In vibration control, the computational methods are focused on individual bearing control, hierarchical schemes for controlling the response of distributed elastic shaft systems and magnetic vibration isolation of space experiment platforms. In dynamic systems, the focus is on new algorithms for structural dynamics analysis.

The Structural Dynamics Branch staff has maintained a tradition of technically excellent work. This will be my last opportunity to report on their accomplishments in an annual report. It has been my sincere pleasure and privilege to have worked so closely with such a dedicated staff of professional engineers and scientists for so many years.

L J Kiraly
Branch Manager

CONTENTS

FORCE ANALYSIS OF MAGNETIC BEARINGS WITH POWER-SAVING CONTROLS

Most magnetic bearing control schemes use a bias current with a superimposed control current to linearize the relationship between the control current and the force it delivers. For most operating conditions the existence of the bias current requires more power than alternative methods that do not use conventional bias. This research examines two alternative methods that diminish or eliminate bias current.

In the typical bias control scheme the desired force output for a harmonic control force command into a voltage-limited transconductance amplifier is obtained only up to certain combinations of force amplitude and frequency. Above these values the force amplitude is reduced and a phase lag occurs. The power-saving alternative control schemes typically exhibit such deficiencies at even lower command frequencies and amplitudes. To assess the severity of these effects, a time history analysis of the force output was performed for the bias method and the alternative methods. The frequency content of the actual force was compared with that of the commanded force. A Fourier series representation (describing function) is used with a concentration on the fundamental frequency component, which is necessary for evaluating the stability of the resulting closed-loop system.

In method A we simulated a strategy in which (for a cosine commanded force) magnet 1 (see fig. 1.) is requested to produce all the force f for f greater than zero; and magnet 2, for f less than zero. Lagging response will be seen to occur near f equal to zero because of voltage railing (saturation). The lag is reduced in method B, which anticipates the zero crossing of force, by initiating current in the opposing magnet when the voltage applied to the operating magnet reaches its limit.

The results show that the methods proposed as power-saving controls use less current than the commonly used bias method but have qualitatively similar effects on force output. The bias has the definite advantage over methods A and B from a linear controls viewpoint in that it has a particular operating range where the force output is not distorted. The force distortion produced in methods A and B possibly can be tolerated and may be of little consequence for some range of operating frequencies.

The power saving that is realized was qualitatively evident from the amount of current flowing in the magnet coils. In the bias case, control current flowed in both magnets almost all the time, in addition to the ever-present bias current. In method A current was commanded in only one magnet at time, but inductive effects caused some overlap. In method B simultaneous currents were actually commanded during a portion of a cycle. Because power loss is related to current, method A would have the least power loss, method B would be next, and the bias method would have the greatest.

Implications as to the effects on stability primarily lie within the amount of phase lag produced. With increased phase lag, stability may deteriorate. The extent of its effect can only be determined by analyzing the closed-loop system with the magnetic bearing and the proposed controls considered herein as elements of the system. The relative amount of phase lag for each method is compared in figure 2.

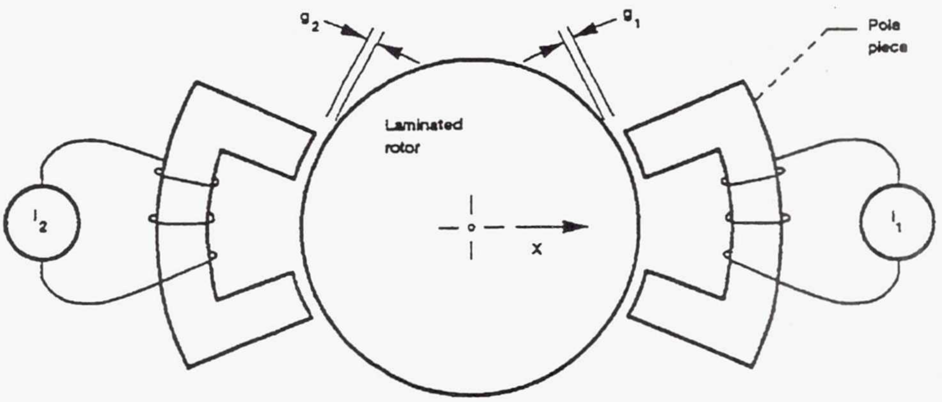

Figure 1. - Diagram of magnetic bearing components operating along a single axis.

In conclusion, the specified methods show some ability as alternative power-saving modes of operation relative to the widely used bias method. Other limitations that were not considered, such as harmonic production, may need to be included in future analyses. Future work will involve proposing and evaluating other alternative methods with more quantitative analysis (e.g., calculated power loss, effect of force harmonics, and response to nonsinusoidal force commands).

Lewis Contact: D. Johnson (216) 433-6046

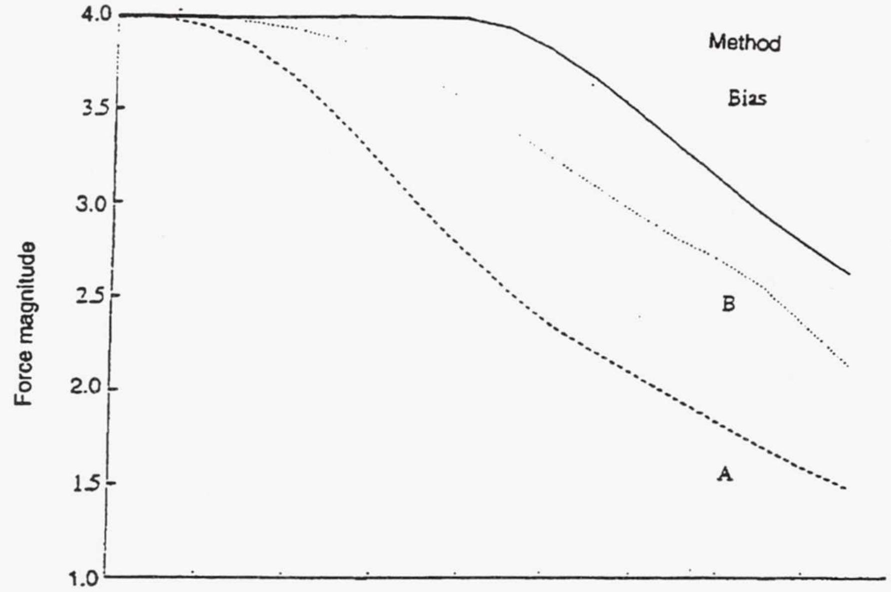

(a) Fundamental Fourier series component magnitude.

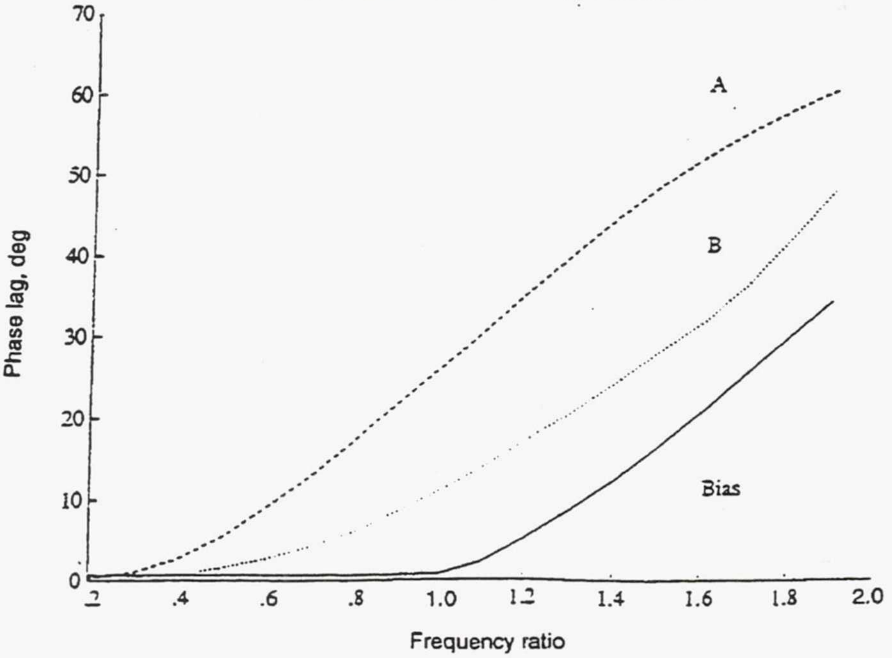

(b) Fundamental Fourier series component phase.

Figure 2. - Describing function for methods A and B and the bias method for a maximum desired force amplitude of 4.

COMBINED PIEZOELECTRIC-HYDRAULIC ACTUATOR-BASED ACTIVE VIBRATION CONTROL

A concept of utilizing piezoelectric actuators to drive hydraulic actuators was conceived in order to fit an output piston into the small envelope adjacent to a gas turbine engine bearing. The output piston of the hydraulic actuator is employed as the primary actuator in the active vibration control system. Early bench tests using hydraulic fluid and ethylene glycol confirmed the viability of the concept. It was suggested to replace the hydraulic fluids with liquid plastic. The gelatin-like texture of the liquid plastic makes it easy to seal, and liquid plastic is reported to have a very high bulk modulus. Many experiment batches of polyvinyl chloride (PVC) and silicone-based plastics are being developed to operate at 350 F. A hydraulic actuator was designed and fabricated for initial tests. Tests have been performed to investigate the effectiveness of the hybrid actuator on an overhung, air-turbine-driven test rig. Details of the installation are shown in figure 1. The piezohydraulic actuators were installed in the horizontal plane only, whereas piezoelectric actuators were installed in the vertical plane but were turned off for the tests. Figure 2 confirms the effectiveness of the hybrid actuator, showing significant reductions in vibration through two modes. The plot is of bearing vibration in the horizontal plane at the actuators. The hydraulic actuators were filled with PVC based liquid plastic for this test. The effectiveness of the actuators was further confirmed by performing transfer function test on them with both oil and liquid plastic. Future work will include testing smaller-tube-diameter transfer lines, developing high-temperature liquid plastic, and testing the devices in other test rigs.

Lewis Contact: A. F. Kascak (216) 433-6024

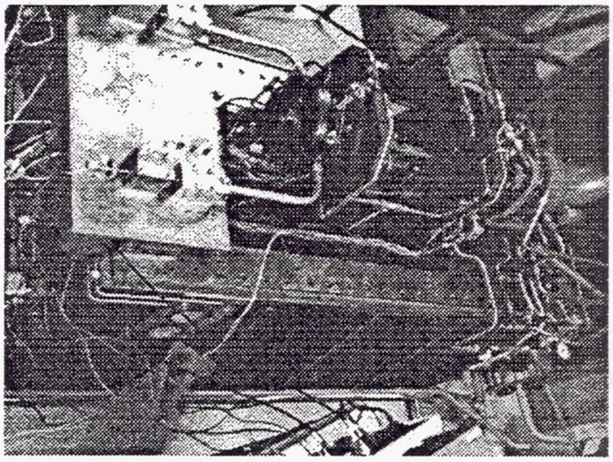

Figure 1. - Hybrid actuator installed in air-turbine-driven test rig.

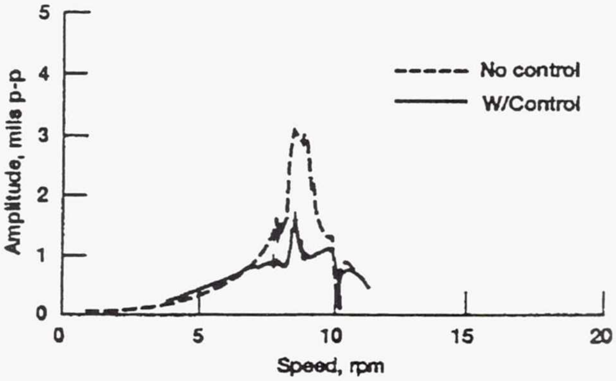

Figure 2. - Vibration of the outboard bearing x plane with and without active control.

Figure 1. - T700 engine test stand at NASA Lewis.

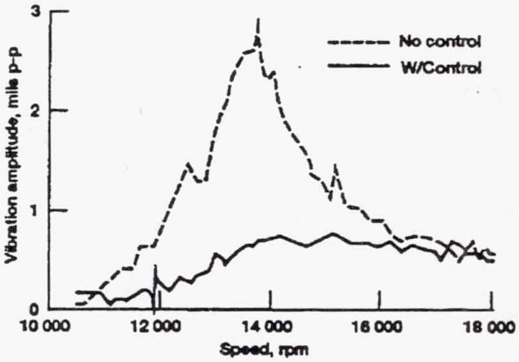

Figure 2. - Vibration response with and without control for sensor y'. Slow roll subtracted.

PIEZOELECTRIC ACTUATOR BASED ACTIVE VIBRATION CONTROL OF TRANSMISSION SHAFT LINE FOR A GAS TURBINE ENGINE TEST STAND

T700 series engines are used in the U.S. Army's utility and attack helicopter fleet. Piezoelectric actuators were installed as part of an active vibration control system on a T701 gas turbine engine test stand (fig. 1). The test stand consists of the engine, a coupling shaft, a spindle that is flexibly mounted on ball bearings, a second coupling shaft, a torquemeter, a gearbox and finally a dynamometer. Piezoelectric actuators apply a control force at the aft end bearing of the spindle shaft. Opposing actuators are aligned in orthogonal axes. Displacement sensors provide feedback signals and are oriented along a second set of orthogonal axes. The signals must be transformed into the coordinate system of the actuators to provide truly collocated feedback. Vibrations were measured at five planes along the shaft line. A analog proportional/derivative (PD) control circuit used a differentiator that had a built-in rolloff to inhibit high- frequency noise. The actuator power amplifiers showed a flat frequency response above 10 000 Hz. The transfer function of the free-tip piezoelectric actuator remains flat to approximately 2000 Hz. Vibrations of the T701 shaft line were suppressed over the entire operating speed range. Test results show that the speedscheduled distribution of active stiffnesses and dampings is most effective in suppressing vibration. Vibration data, with and without control, are shown in figure 2 at eight eddy current displacement probes on the shaft. In addition to the PD analog feedback, test results were obtained by using digital signal processing (DSP) active control.

Researchers: A. F. Kascak (216) 433-6024

TESTS OF CRYOGENIC MAGNETIC BEARING WITH PERMANENT-MAGNET BIAS

The cryogenic turbopumps for pumping liquid hydrogen and liquid oxygen to the Space Shuttle main engines (SSME) have experienced serious rotor vibrations, and the bearings have very short life. It appears that the vibration problems and short bearing life can be addressed by using magnetic bearings. A magnetic bearing that utilizes both permanent magnets and electromagnets was tested at room temperature and in liquid nitrogen at -320 °F. The bearing built for this study was 5.25 inches in diameter and 4.5 inches long and weighed 17.4 lb. The bore was 3.03 inches and the air gap was 0.024 inch. The radial load capacity of 500 lb could be substantially increased by optimization.

The objectives of the tests were as follows:

(1) To determine the feasibility of using magnetic bearings in cryogenic turbopumps

(2) To apply magnetic bearings to control the rotordynamics of supercritical rotors such as those found in the SSME turbopumps

(3) To explore any special problems in applying magnetic bearings to turbopumps

The test rig shown in figure 1 simulates a rotor and the cold environment of a cryogenic turbopump. It has a unique capability of applying measured forces to the shaft to measure magnetic bearing stiffness and permanent-magnet forces at both room temperature and liquid nitrogen temperature. The rotor, which has a vertical axis, is supported by the magnetic bearing at the bottom and a preloaded duplex ball bearing at the top. The magnetic bearing carries only radial load, but the ball bearing carries both radial and thrust loads. The rotor is driven by an ac motor through a belt-and-pulley speed increaser (2:1 ratio) at speeds up to 14 000 rpm. The rotor has two critical speeds within the operating range. The mode shapes are conical (with some bending) and first bending. The rotor can be unbalanced by placing set screws in one of the disks. For cryogenic operation, liquid nitrogen at -320 °F submerges the magnetic bearing.

The key magnetic bearing components can be seen in figure 1. These are the ferromagnetic rotor, the rotor laminations, the stator laminations, the stator windings, the samarium cobalt permanent magnet, the pole piece, and the position sensors. The backup bearings shown at the bottom of the shaft positions the rotor when the magnetic bearing is not operating. When the rotor is centered, there is a 0.010-in. radial gap between the rotor and the backup bearing.

A simple proportional, integral, derivative (PID) analog controller was designed and used to control the bearing during the tests. The schematic of the control circuit for one bearing axis is shown in figure 2. The component values shown produced a measured stiffness of 20 000 to 22 000 lb/inch. The derivative was limited to a 1.5-kHz bandwidth, and the overall control was limited to a 3-kHz bandwidth by the low-pass filter.

Linear transconductance power amplifiers were used for the tests. The resistive-capacitive feedback circuit, which is required for stability, limits the bandwidth of the amplifier to about 1.5 kHz.

Rotating tests were performed for magnetic bearing stiffnesses from 10 000 to 22 000 lb/inch at room temperature and liquid nitrogen temperature and for 46 000 lb/inch at room temperature. The rotor was finely balanced for these tests (i.e., no intentional unbalance was applied). For a magnetic bearing stiffness of approximately 20 000 lb/in., the bearing was operated up to 14 000 rpm, which is the full speed capability of the rig. Two critical speeds were traversed, a primarily conical mode at 6300 rpm and a first bending mode at 12 600 rpm.

This magnetic bearing differs from early hybrid designs by avoiding placement of the electromagnets and the permanent magnets in a disadvantageous simple-series magnetic circuit. The particular way in which this is done results in a "homopolar" geometry. An advantage of the homopolar geometry is that the field excursions experienced by the rotor are reduced in frequency and magnitude, reducing rotor heating by magnetic hysteresis and by eddy currents.

These tests have shown that it is feasible to use the hybrid magnetic bearing in the cryogenic environment and to control the rotordynamics of flexible shafts when operating at or above the bending critical speeds.

Although this hybrid magnetic bearing is much smaller and lighter than commercial magnetic bearings, for turbopump applications the size and weight should be reduced further. This can be achieved through optimization of the present design. Also the control system must be developed to improve the stability margin at higher bearing stiffness.

Lewis Contact: E. DiRusso (216) 433-6027

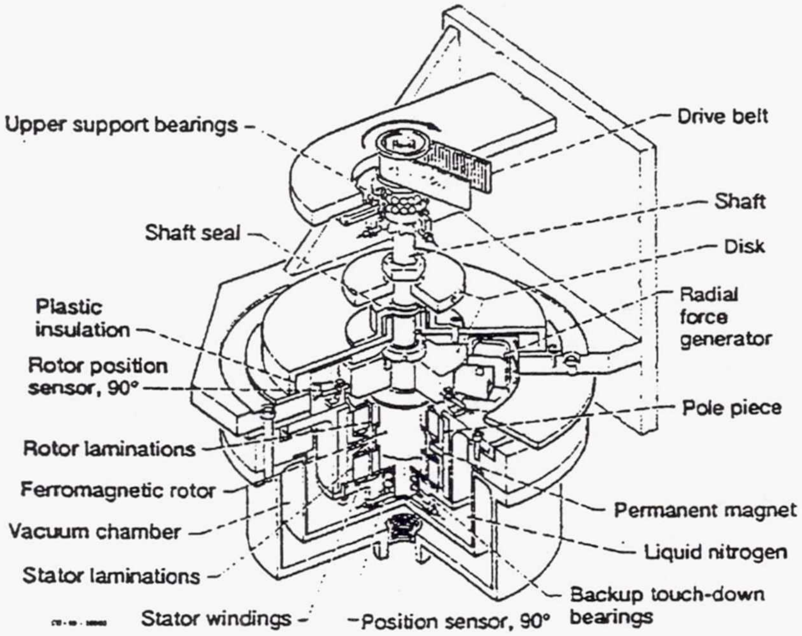

Figure 1. - Cryogenic hybrid magnetic bearing and test rig.

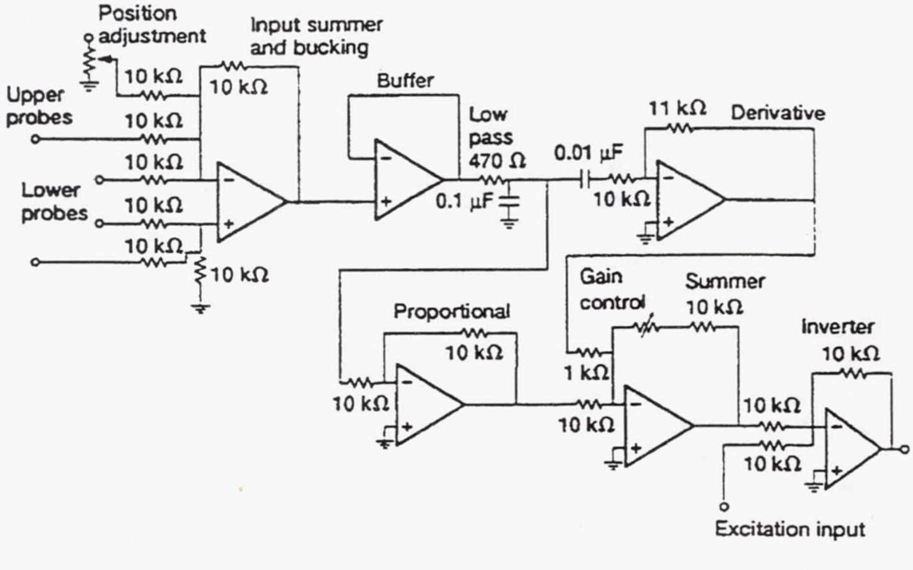

Figure 2. - Analog control system for hybrid magnetic bearing.

MAGNETIC BEARINGS FOR FREE-PISTON STIRLING ENGINES

A study has shown that magnetic bearings are feasible for the power pistons of the reference Stirling space power converter (RSSPC), a 50-kWe free-piston Stirling engine for converting thermal energy into electrical energy. Use of magnetic bearings can increase the net power output of the RSSPC by about 370 W, or 0.7%. Magnetic bearings will also increase the mass by 14 kg, or about 5%.

The current RSSPC is equipped with hydrostatic (pressurized) helium gas bearings to support the reciprocating power pistons without sliding contact. A disadvantage of this arrangement is that pressurized helium is not immediately available at engine startup; the RSSPC bearings must operate with sliding contact during startup. In addition, very small radial clearances (13 to 18 μm) are required to minimize the power used to pressurize the bearings. Even with these small clearances, the power required for the power piston bearings represents 1.1% of lost electrical output.

Magnetic bearings have the potential to eliminate these disadvantages. Magnetic bearings have very low losses, leading to improved overall system efficiency. They can be electrically energized (levitated) at any time, whether or not the RSSPC is operating. Also, magnetic bearings can be designed with order-of-magnitude larger clearances than are required for gas bearings. This greatly reduces the problem of maintaining safe bearing clearances in the presence of differential thermal expansions, and also makes the bearings less susceptible to debris.

An eight-pole (four-sector) attraction-force active magnetic bearing with electromagnetic bias was designed for the RSSPC. It consists of two electromagnets per axis placed on opposite sides of the rotor. Maximum flux density was taken to be 1.8 T; this corresponds to the use of high-saturation-flux iron-cobalt-vanadium alloys for all the magnetic materials. The zero-eccentricity air gap for all electromagnets was specified to be 130 μm, which is 5 to 7 times the radial clearance of the piston seals. Figure 1 shows a cross section of the magnetic bearing assembly. The eight bearing electromagnets are mounted inside the bore of the piston via an arbor that is bolted to the end of the power piston cylinder.

Lewis Contact: D. P. Fleming (216) 433-6013

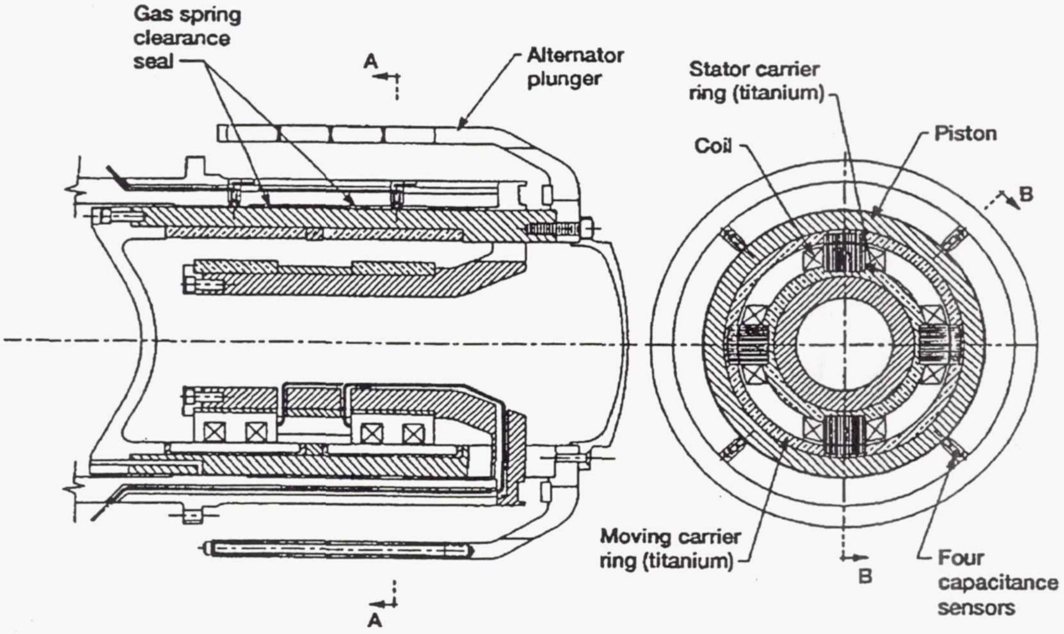

Magnetic bearing assembly for RSSPC power piston.

INVERSE KINEMATICS PROBLEM IN ROBOTICS USING NEURAL NETWORKS

Single and multilayer feedforward networks were applied to the robot inverse kinematic problem. The networks were trained with end-effector position and joint angles. After training, performance was measured by having the network generate joint angles for arbitrary end-effector trajectories. A three-degreeof-freedom (DOF) spatial manipulator was used for the study. Neural networks provided a simple and effective way both to model the manipulator inverse kinematics and to circumvent the problems associated with algorithmic solution methods.

Solving the problem using the conventional programmed approach requires the development of software to implement the algorithms or sets of rules. Frequently, such as for nonlinear or complex multivariable systems, the sets of rules or required algorithms are too complex to be accurately modeled. Even if characterizing algorithms are obtained, they often are too computationally intensive for practical real-time applications. To circumvent these problems, a relatively new approach to information processing known as neurocomputing has been developed. This approach, which does not require algorithm or rule development, is advantageous because it may significantly reduce the quantity of software development, decrease computational requirements, and allow for information-processing capabilities where algorithms or rules are not known or cannot be derived.

This study explored the application of a neural network for approximating the nonlinear transformation relating the manipulator's end-effector position to its joint coordinates. Among a variety of neural networks, two networks were chosen for the present study: single hidden layer and multiple hidden layer feedforward networks. The multilayer network was chosen because of its enhanced capability to model nonlinear system characteristics. The networks were trained by using the end-effector position of a three-degree-of-freedom manipulator as input and its corresponding joint angles as output. After the network was trained, end-effector positions that were not part of the original training data set

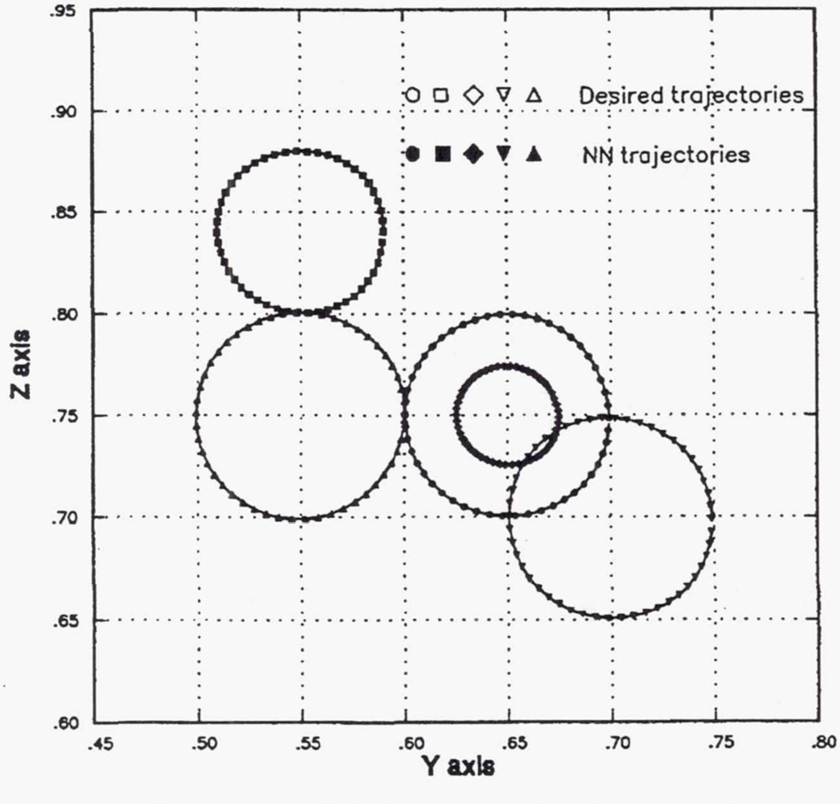

Figure 1. - A 2-10-10-2 network using 73 training points.

were input to the network to assess its capabilities for generating correct joint angles for arbitrary end-effector positions.

Figure 1 shows the 2-10-10-2 network's capabilities for producing planar circular trajectories learned with 73 training points. Clearly, this network is able to accurately generate joint angles for end-effector positions anywhere within the workspace. In fact, the joint angles accuracy is within 1% rms (root mean square) for any of the trajectories.

Figure 2 was created by training the network with 27 training points and then having it generate four spacial arbitrary trajectories. The network was able to map each of the four trajectories to within 2% rms accuracy.

Considering the success of the neural network for solving the inverse kinematic problem, future studies may address the application of neural networks for solving the redundant manipulator kinematic problem where minimal base reactions are desired.

Lewis Contact: B. B. Choi (216) 433-6040

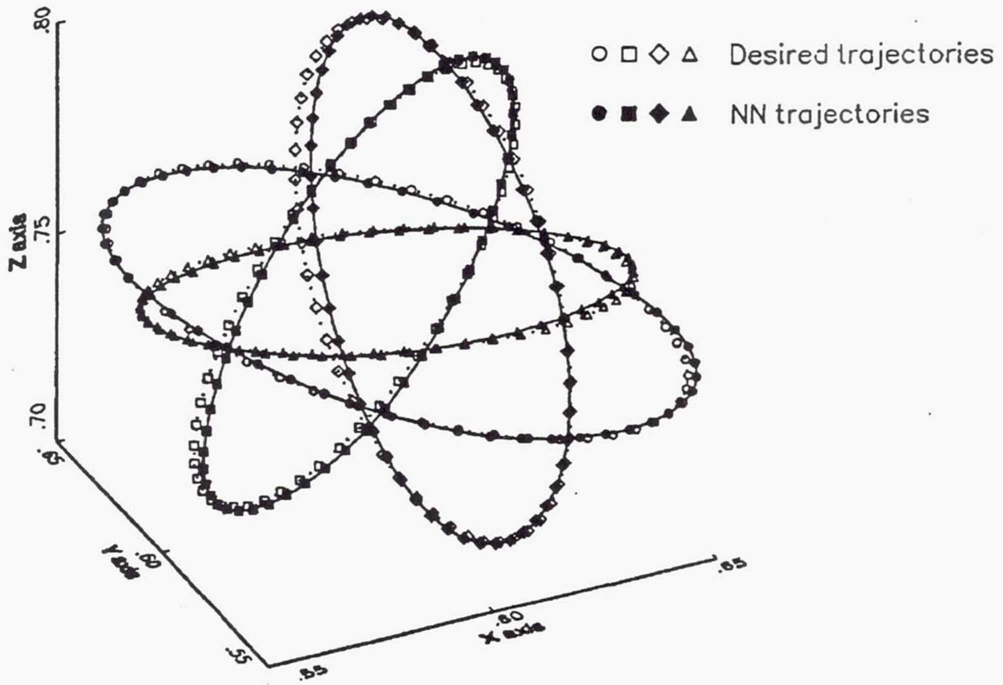

Figure 2. - A 3-10-10-3 network using 27 training points.

HIGH-TEMPERATURE DYNAMIC ENGINE SEAL TECHNOLOGY DEVELOPMENT

Combined-cycle ramjet/scramjet engines being designed for advanced hypersonic vehicles, including the National Aerospace Plane (NASP), require innovative high-temperature dynamic seals to seal the sliding interfaces of the articulating engine panels. New seals are required that will operate hot (1200 to 2000 °F), will seal pressures ranging from 0 to 100 psi, will remain flexible to accommodate significant sidewall distortions, and will resist abrasion over the engine's operational life. NASA Lewis is developing advanced seal concepts and sealing technology to meet these demanding seal challenges.

The current study reviews the recent high-temperature durability screening assessments of the braided ceramic rope seal concept, which is braided of emerging high-temperature materials. The current work presents durability data for: (1) the fundamental seal building blocks, a range of candidate ceramic fiber tows; and for (2) braided rope seal subelements that were scrubbed under engine simulated sliding, temperature, and preload conditions.

Alternative fiber durability tests were run to assess the relative sliding durability of a range of candidate ceramic materials under both air and hydrogen environments. Tests were run at room temperature, 930 °F, and 1650 °F. These tests demonstrated the deleterious effects on the high-temperature sliding durability of Nextel 312 and 440 caused by heat treating the fibers at 1750 °F for 12 hr. This heat treating or material conditioning is recommended by the manufacturer to improve fiber resistance to steam environments. Unfortunately, this preexposure temperature falls well within the intended seal operating temperature. The tow durability tests also revealed the encouraging result that a new fiber, Nextel 550 (Al_2O_3-SiO_2), was not degraded by this temperature preexposure. A second sequence of tow durability tests with the same fibers were run in hydrogen at the same three temperatures. These tests showed that the oxide ceramic fibers exhibited somewhat better sliding durability in hydrogen than in air at temperature.

The relative sliding durability of a range of seal subelement architecture/material combinations were assessed in a joint program between NASA, Pratt & Whitney, and Drexel University. The high-temperature durability of five different braided rope seals were assessed. Only the hybrid braided rope seals (M1 and M2 in the Fig.), which have a metal sheath braided over a dense uniaxial ceramic core, survived the full 2000-cycle duty cycle. Although the all-ceramic seals (M4a to M6 in the Fig.) exhibited lower leakage rates than the hybrid seals, the all-ceramic seal sheaths were severely damaged after only 14 to 42% of the duty cycle. The hybrid seals also exhibited lower friction at temperature, a key for smooth engine panel articulation.

On the basis of the results obtained, the hybrid architecture will be further optimized to exploit its excellent durability and low friction while reducing leakage flow rates. These seal development/optimization studies will be performed in a new high-temperature dynamic seal test rig under development at NASA Lewis. This fixture will be used to assess the change in seal leakage versus wear cycles at engine simulated temperatures up to 1500 °F, pressures up to 100 psi, and sliding velocities up to ± 1 in./sec.

Researcher: B. M. Steinetz (NASA Lewis)

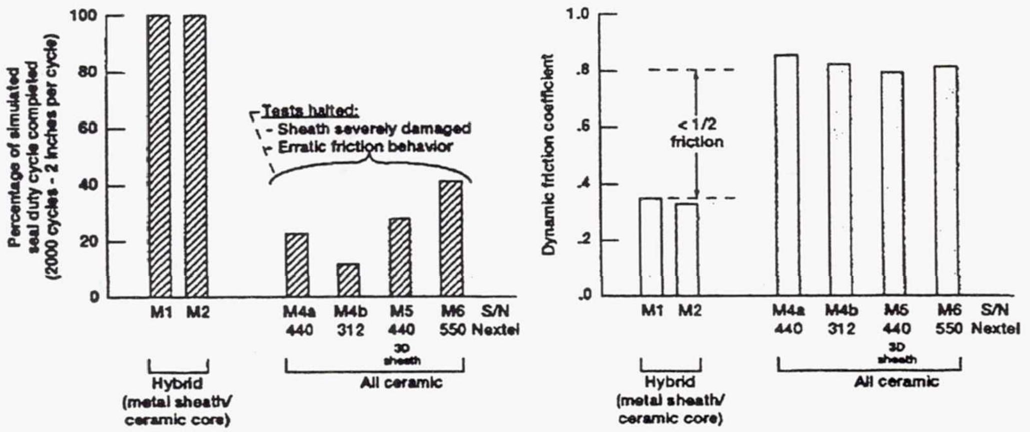

Comparison of solid seal dynamic performance at 1300° F.

ENGINE PANEL SEALS FOR HYPERSONIC ENGINE APPLICATIONS: HIGH-TEMPERATURE LEAKAGE ASSESSMENTS AND FLOW MODELING

Combined-cycle ramjet/scramjet engines being designed for advanced hypersonic vehicles, including the National Aerospace Plane (NASP), require innovative high-temperature dynamic seals to seal the sliding interfaces of the articulating engine panels. New seals are required that will operate hot (1200 to 2000°F), will seal pressures ranging from 0 to 100 psi, will remain flexible to accommodate significant sidewall distortions, and will resist abrasion over the engine's operational life. NASA Lewis is developing advanced seal concepts and sealing technology to meet these demanding seal challenges. Two seal designs that show promise of meeting the demanding operating conditions of the NASP engine environment and sealing the gaps between the movable horizontal panels and the vertical splitter walls are the ceramic wafer seal and the braided ceramic rope seal.

Key elements of leakage flow models for each of these seal types have been determined. Flow models such as these help designers to predict performance-robbing parasitic losses past the seals and to estimate purge coolant flow rates. The leakage model developed for the ceramic wafer seal was based on the theory of externally pressurized gas film bearings, which was modified to account for the special features of the seal. The Reynolds flow equation was used as the basis of the flow equations to account for each of the three potential leakage paths: past the nose of the seal; around the back side of the seal; and at temperature, between the wafer elements. The braided rope seal leakage model was based on Kozeny-Carmen relations for flow through porous media. The model treats leakage flow through and around the braided seal structure as a system of flow resistances that are analogous to a series of resistors in an electrical network. These elemental resistances are combined in accordance with their electrical analog to form an overall effective seal resistance that characterizes the seal.

A specially developed high-temperature seal rig was used to collect the required leakage flow rates for validating the seal leakage flow models, as a function of simulated engine temperatures (up to 1350°F), pressures, and preloads.

As shown in the figure, the correlation between the measured and predicted leakage rates for the ceramic wafer seal was quite good over the full temperature range examined. Note that the wafer seal met the tentative leakage limit (shown by the dashed horizontal line) over the measured temperature range. The correlation between the measured and predicted leakage rates for the braided ceramic rope seal was good considering the difficulty in modeling flow through these porous seal structures. At room and moderate temperatures the rope seal model somewhat overpredicted the leakage rate, resulting in a conservative estimate of leakage flow. Work in progress is investigating the effect of preload and engine pressure on seal flow resistance, which may explain part of the noted discrepancy.

Lewis Contact: B. M. Steinetz (216) 433-3302

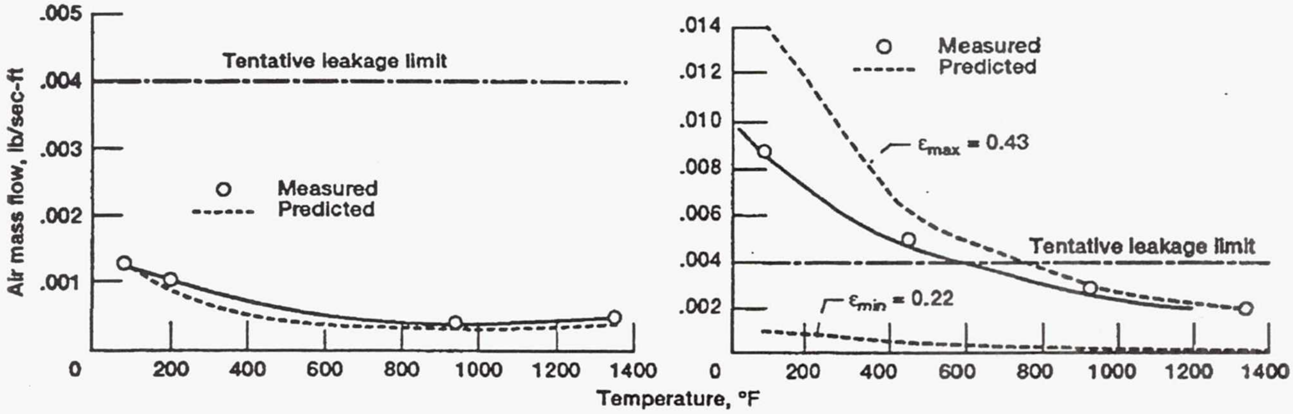

(a) Ceramic wafer seal correlation. ΔP = 40 psi.

(b) Braided ceramic rope seal correlation. ΔP = 35 psi.

Seal leakage flow modeling.

DYNAMIC EFFECTS OF INTERNAL ROBOTS ON SPACE STATION FREEDOM

Many of the planned experiments for Space Station Freedom will require acceleration levels to be no greater than microgravity (10^{-6} g) levels for long periods of time. Studies have demonstrated that without adequate control, routine operations may cause disturbances which are large enough to affect onboard experiments. One way to both minimize disturbances and make Freedom more autonomous is to utilize robots instead of astronauts for some operations. Two methods for minimizing the dynamic disturbances resulting from the robot motions were evaluated. The first method is to use a robot with kinematic redundancy (redundant links). The second method involves using a vibration isolation device between the robot and the laboratory module.

Kinematic redundancy has been shown to reduce the disturbance levels for a typical robot motion from 4.7 μg to less than 1 μg (fig.). The effectiveness of the vibration isolation devices (VID) was shown to be dependent on their natural frequency. As the isolator frequency increased, their effectiveness decreased and the transmitted acceleration became quite large. Soft or low-frequency isolators were effective in reducing acceleration levels, but the resulting displacement at the robot base became prohibitively large.

A tunable VID was then compared with the passive VID having fixed parameters. For stiff isolators with displacements of less than 5 cm (2 in.) the fixed and tunable isolators delivered comparable results. For flexible isolators with displacements greater than 40 cm (16 in.) the disturbance level was small, and fixed and tunable isolators again produced equivalent results. In the range 5 to 40 cm (2 to 16 in.) the tunable isolator was more effective in minimizing the transmitted reactions.

It was also shown that redundant robots may allow heavy payload experiments to take place without disturbing the microgravity environment. These experiments would cause large disturbances without reaction compensation because the payload itself, not the actuating system, is causing the disturbances. The robot is able to compensate not only for itself but also for the disturbance caused by the payload motion.

Kinematic redundancy and vibration isolation can both be used to reduce disturbance forces.

Researchers: J. H. Miller (Sverdrup Technology, Inc.); C. Lawrence and D. A. Rohn (NASA Lewis)

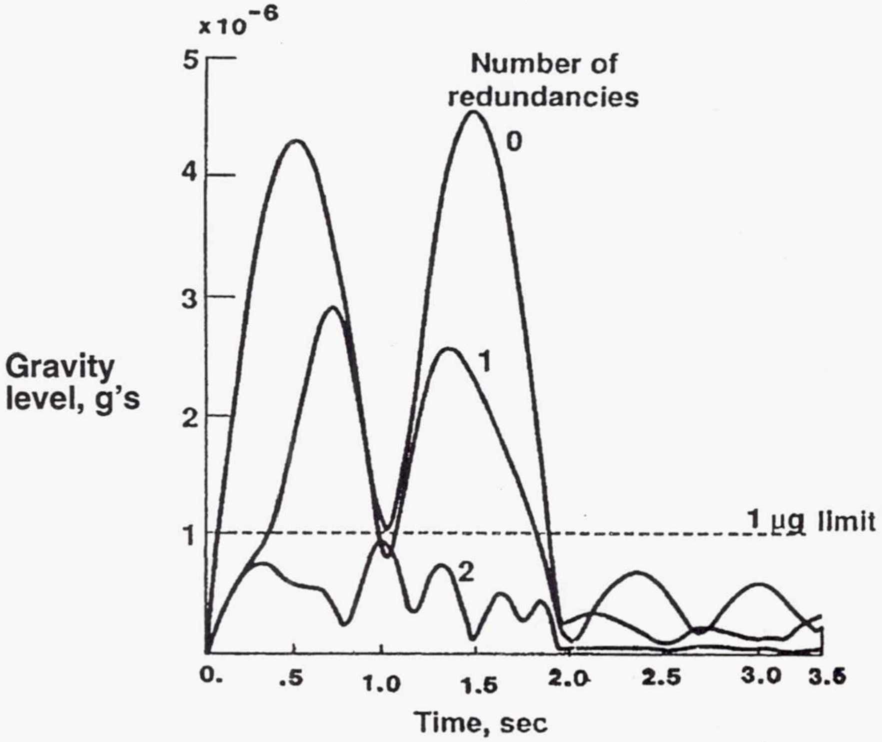

Acceleration level comparison.

DETRIMENTAL EFFECT OF FRICTION ON SPACE MICROGRAVITY ROBOTICS

The desire to perform acceleration-sensitive experiments in space has uncovered a problem that is common to all current state-of-the-art robot systems. The presence of Coulomb friction in a robot's drive train limits smoothness of motion, and feedback control is not effective in achieving higher smoothness. An analysis of why control systems are ineffective in compensating for acceleration disturbances due to Coulomb friction was performed. Linear arguments indicate that the effects of Coulomb friction in a body are most difficult to reject when the control actuator is separated from the body by a compliance. Our linear arguments were illustrated in a nonlinear simulation of optimal linear tracking control in the presence of nonlinear friction (fig. 1). Endpoint acceleration measurements were made for four different robot designs and compared with our simulation and with equivalent measurements on a human (fig. 2). We concluded that Coulomb friction in common bearings and transmissions induces unacceptable levels of endpoint acceleration, that these accelerations cannot be adequately attenuated by control, and that robots for microgravity work will require special design considerations for inherently low friction.

***Researchers:* W. S. Newman and G. D. Glosser (Case Western Reserve University); J. H. Miller (Sverdrup Technology, Inc.); D. A. Rohn (NASA Lewis)**

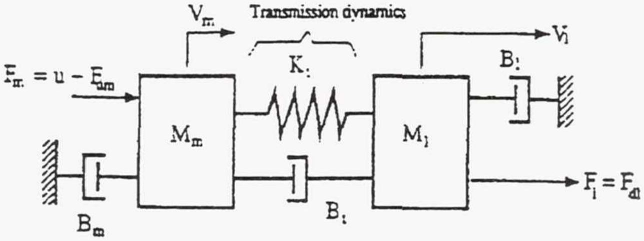

Figure 1. - Robot joint dynamic model.

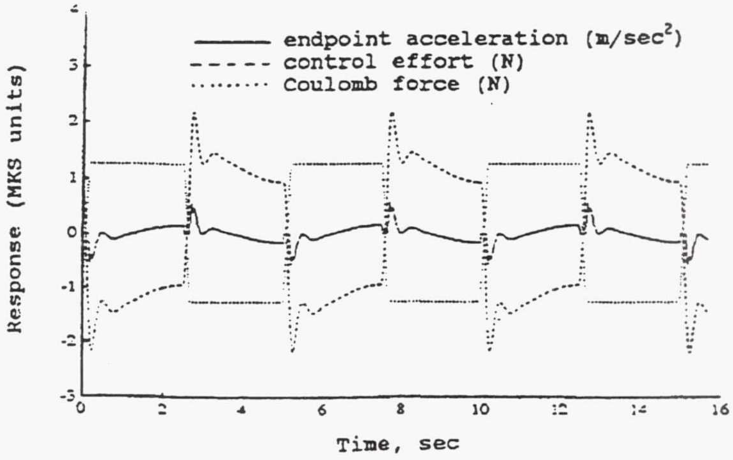

Figure 2. - Results of simulation in presence of Coulomb friction.

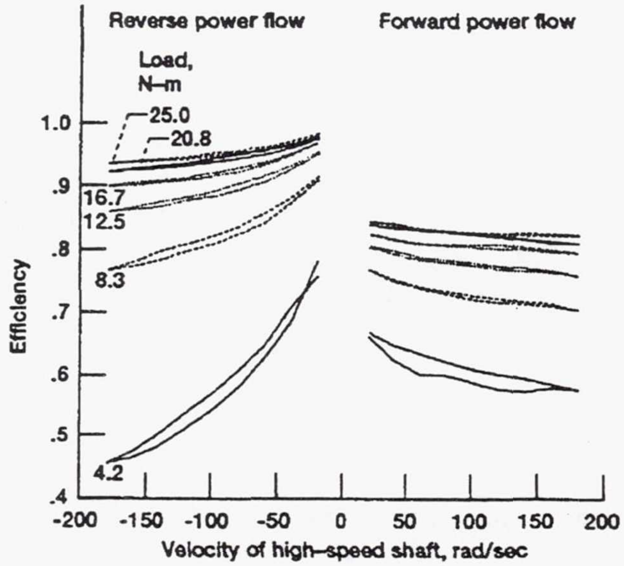

Efficiency of four-planet, 23.2:1 ratio, roller-gear drive with high-speed velocity source and low-speed torque source.

DESIGN AND TESTING OF A 23.2:1 RATIO, PLANETARY ROLLER-GEAR ROBOTIC TRANSMISSION

Robotic manipulator systems have been proposed for an increasing variety of tasks in space. Like all servomechanism systems, robotic arm actuators require high-performance mechanical power transmissions. Requirements include high efficiency, linearity, low backlash, low torque ripple, and low friction.

A single-axis transmission that utilizes rollers and gears acting in parallel was designed for a robotic manipulator. Traction drives offer the advantages of high efficiency at high ratios, backlash-free operation, low noise, no gear cogging, smooth torque transfer, and back-drivability, but they are torque limited. The maximum tangential force that can be transmitted through a roller contact is a function of the normal load and the available traction coefficient. Where the torque to be transmitted exceeds the capability of a pure traction drive, roller-gear arrangements offer an alternative approach. The gears enhance torque capacity. The rollers provide positioning for the gears, allow the use of multiple planet rows, remove backlash from the torque path, attenuate gear cogging and torque ripple, and support the radial component of gear tooth forces.

The design of a cluster configuration for a traction drive presents a few constraints because an almost infinite array of roller arrangements can be conceived to fit within a given circle. The introduction of gears with finite numbers of teeth to function in parallel with the rollers, however, imposes severe limits on available designs. Solutions for two planet row designs are discussed. Gear design must be carefully matched with rollers to ensure good kinematic action. Compromises in tooth design to accommodate mismatching, which occurs in the best of solutions, need to be made.

Roller action in roller-gear drives is such that, at startup before the gears are fully meshed, the compressively loaded rollers transmit torque. "Creep" or loss of motion occurs in rollers transmitting torque; this causes the gears to "catch up" and assume the burden of torque transmission. Thus the role played by rollers in torque transmission is transitory.

Iterative calculations of roller torque fraction, normal load and Hertzian contact are made to determine a feasible level of torque that can be carried through the rollers. In this design, a torque fraction of 0.20 was settled upon as reasonable for the rollers.

A two-planet-row, four-planet design was conceived and two assemblies, one all steel and one containing alternate steel and plastic rollers and gears, were fabricated and tested. Detailed calculations of cluster geometry, gear stresses, gear geometry, and measurement data are given. Gear tooth geometries necessary for manufacture and data required for inspection were developed.

Measurement data included transmission linearity, static and dynamic friction, inertia, backlash, stiffness, and forward and reverse efficiency. Transmission linearity was measured to within 0.001°. Friction was measured by using reactionless rotating torque transducers as a function of input speed, with the transmission operating both as a speed reducer and as a speed increaser. Inertia was determined through sinusoidal excitation experiments. Backlash was not measurable, but less than 0.001° with respect to the output angle. Stiffness measurements indicated that the transmission behaved as a "stiffening spring," with stiffness increasing with load.

Efficiency measurements taken were unusually complete (see figure). The transmission was loaded by controlled actuators at both the high-speed and low-speed shafts. Power transfer efficiency was measured in four regimes: (1) controlled velocity source on the high-speed shaft, controlled torque source on the low-speed shaft, and power flow from high speed to low speed (conventional measurement, speed-reducer operation); (2) controlled velocity source on the low-speed shaft, controlled torque source on the high-speed shaft, and power flow from low speed to high speed (speed-increaser operation); (3) controlled velocity source on the low-speed shaft, controlled torque source on the high-speed shaft, and power flow from high speed to low speed (torque increaser operation); and (4) controlled velocity source on the high-speed shaft, torque source on the low-speed shaft, and power flow from low speed to high speed (torque reducer operation). An unusual result of the measurements was that the "back-driven" operating modes of torque reducer and speed increaser resulted in higher efficiencies than the normal "forward" operating modes (speed reducer, torque increaser). Peak efficiency was 98.5%, occurring at low speed and maximum torque with power flow in the "reverse" direction (from low-speed shaft to high -speed shaft).

Lewis Contact: D. A. Rohn (216) 433-3325

STRUCTURAL CONCEPTS FOR A MULTIMEGAWATT SOLAR ELECTRIC SPACECRAFT

As a part of the Space Exploration Initiative (SEI), NASA is investigating scenarios for a mission to MARS. In support of this effort, NASA Lewis is studying a solar electric propulsion (SEP) spacecraft to be used as a cargo transport vehicle to MARS. Structures are particularly important for SEP vehicles because of the large surface areas that must be supported to accommodate the solar power systems. As a result, the spacecraft structure greatly influences the overall spacecraft design and weight.

The SEP structure will be designed to meet stress and stiffness requirements with the overall design objective being minimum weight. These spacecraft structural designs will be influenced more by stiffness requirements, whereas previous designs often have been dictated by stress limitations. In the past the most severe loads that a spacecraft, which was entirely constructed on Earth, was exposed to were a result of the launch environment. On-orbit loading was significantly less demanding. The SEP spacecraft will be deployed, or constructed, in space and the loading situations will be considerably more complex. Although the structural integrity of the packaged spacecraft components may be most influenced by the launch environment the completed spacecraft will be affected only by on-orbit (or in-flight) loadings. Furthermore, because the loadings in space generally are very small, stiffness rather than stress limitations probably will dominate the structural design. Actual construction of the SEP will present another challenging problem. Because of the SEP's large size, unique construction methods will have to be devised. The structure may be constructed by exacting deployment schemes, by in-space erection methods, or most probably, by a combination of both.

Two preliminary structural design concepts were investigated for the SEP spacecraft: a split-blanket array configuration, and a ring structure. Both designs were assessed by comparing their overall weights, stiffnesses, and performance under loadings.

The first structural concept is based on an segmented, octagonal split-blanket configuration. The main components of each octagonal segment are a central mast for supporting thrusters and upper and lower crossbooms. Split-blanket arrays are stretched between the crossbooms. This configuration is similar to previously developed designs such as the Space Station Freedom photovoltaic solar arrays. The second structural concept is based on a circular design that was originally proposed for very large solar concentrators (see figure). The design consists of a central mast that extends perpendicular to the solar blankets and an outer ring truss structure that is suspended by guy wires. The solar blanket is stretched inside the ring truss. The ring structure configuration has several advantages over the split-blanket structure. For a fixed quantity of available structure the ring structure is orders of magnitude stiffer, it is more stable as a result of shorter compression members, and it deflects less and has less stress as a result of operating loadings. The only identified disadvantage of the ring configuration is that it may be more difficult to deploy or construct in space.

Lewis Contact: C. Lawrence (216) 433-6048

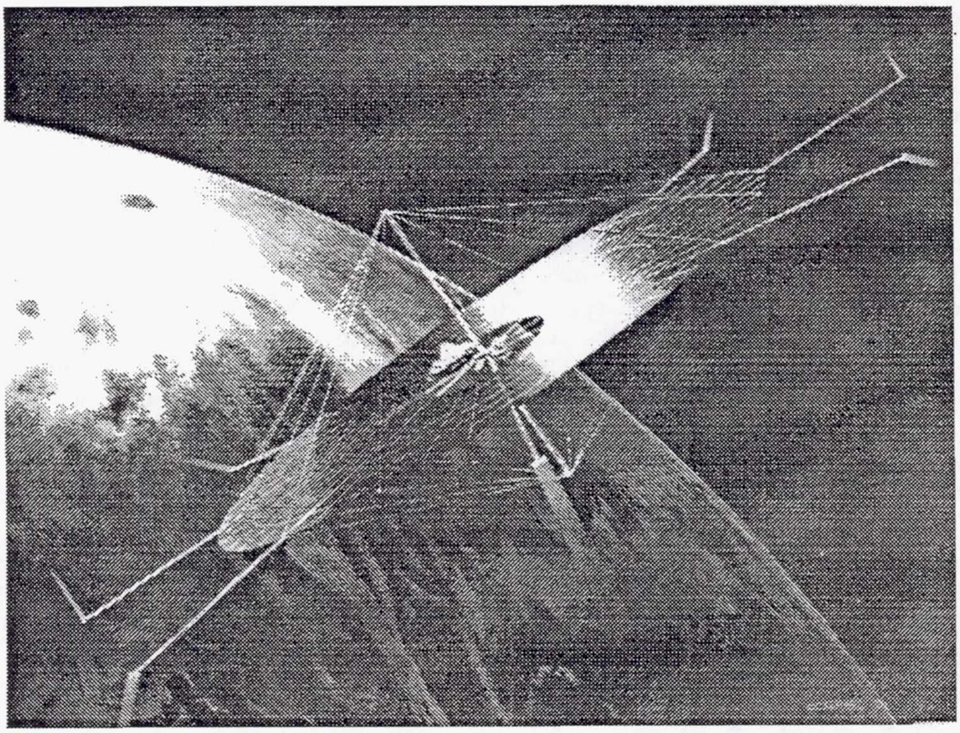

Ring configuration for solar-electric-powered spacecraft.

PARALLEL, NONLINEAR STRUCTURAL DYNAMIC SIMULATIONS OF ROTATING BLADED-DISK ASSEMBLIES USING OF NETWORKED WORKSTATIONS

With the increasing availability of workstations in the workplace, engineers may be able to take advantage of a network of these workstations to achieve improved turnaround through parallel computations for computationally intensive simulations such as nonlinear dynamic analyses.

Research is ongoing on parallel solutions of nonlinear structural dynamics in a distributed-memory, coarse-grained parallel processing environment consisting of networked engineering workstations. Both numerical algorithms for parallel, nonlinear solutions and techniques to effect load balancing among processors are investigated in this research.

The principal problem selected to be studied is the structural dynamics of rotating turbine bladed disk assemblies that experience tip rubs.

The current parallel-processing, environment consists of up to sixteen HP9000/720's. Each HP9000/720 has 64 megabytes of memory and a central processor running at the speed of approximately 59 Mips. These workstations utilize the UNIX operating system, are connected by Ethernet, and communicate via TCP/IP. Any processor may communicate directly with any of the other processors.

In this implementation of coarse-grained parallel processing, the structure is first partitioned into a number of substructures. The computations for each substructure are then handled by one processor, and the number of finite elements in the structure is usually much larger than the number of substructures (processors).

The finite element approach is employed to model the complex structural geometry and material properties of the bladed disk, to formulate governing equations of motion for the problem, and to account for various nonlinearities involved in the problem. An example of a finite element bladed-disk model with simplified geometry is shown in the figure. This model consists of 504 solid hexahedral elements and 1488 nodes. Because turbine blades are relatively flexi-

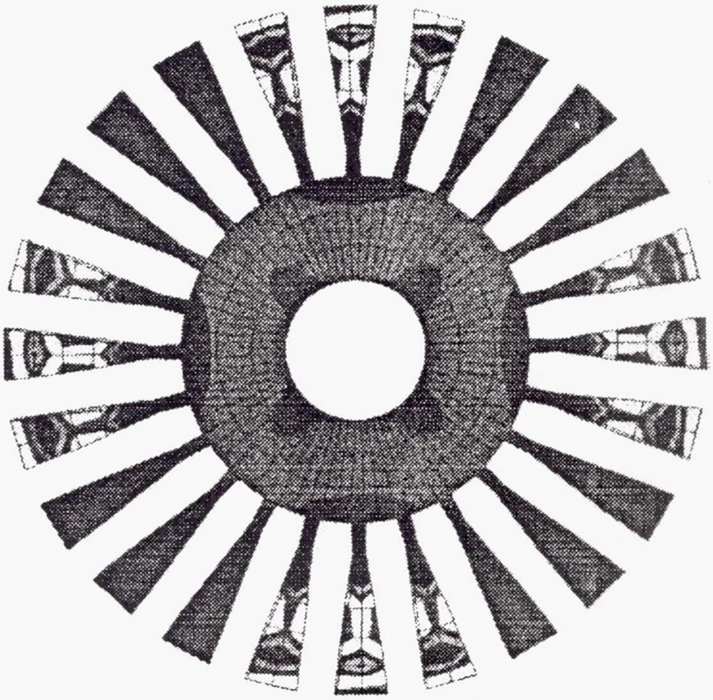

Blade disk assembly.

ble and normally respond to the centrifugal forces with considerable deflections, a geometric nonlinear analysis is usually required for accurately predicting the dynamic behavior of rotating blades. The governing equations of motion derived from the finite element approach have the form

$$[M]\{Q\}+[C_s]+[C_c])\{Q\}+([K_e]+[K_g]+[K_a]-[K_r])\{Q\}+\{F_e\} = \{F^{ext}\}$$

in which, $[M]$, $[C_s]$, $[K_e]$, $[K_g]$ are the mass, structural damping, elastic stiffness, and geometric stiffness matrices, respectively, $(C_c]$, $[K_a]$, and $[K_r]$ are the Coriolis damping, centripetal stiffness, and centrifugal stiffness matrices, respectively, resulting from the rotational effect, $\{F^{ext}\}$ is the external force vector, and $\{F_e\}$ is the rotational force vector. The computation of these rotation-related terms is expensive (each has about the same amount of computation as the stiffness matrix formation).

For steady-state solutions of the rotating bladed-disk model a parallel static algorithm has been implemented. The algorithm performs a substructuring procedure that uses a parallel, preconditioned, conjugate gradient algorithm for the iterative solution of the reduced set of unknowns along the substructure interfaces.

For transient solutions a parallel, explicit algorithm using the central difference method has been implemented. The central difference method is conditionally stable and is inherently amenable to parallel processing. With standard selections of the finite difference relations and the use of lumped masses, the solution may proceed on a degree-of-freedom level without the assembly of the global stiffness matrix the solution of simultaneous equations. In addition, with appropriate preparation of substructure data for each processor, a minimum amount of interprocess communication may be achieved between adjacent processors.

The parallel finite element analysis system implemented involves three in-house, general-purpose programs, a three-dimensional modeling and visualization program named FRANSYS; an interactive, parallel, structural analysis interface named PSAINT; and a batch analysis program named ABREAST for the solution of nonlinear structural dynamics. FRANSYS provides the analyst an efficient way of modifying and manipulating the structural data through the use of a topological representation. It also provides a convenient means of displaying the structure model and visualizing the dynamic response of the structure by using interactive computer graphics. PSAINT has capabilities of performing domain partitioning for parallel analysis and collecting analysis results for FRANSYS from various processors for monitoring the progress of parallel simulations. ABREAST is originally geared toward frame structures consisting of either truss or beam-column elements. It is capable of both geometric and material nonlinear transient dynamic analyses. For modeling bladed-disk assemblies a 20-noded, isoparametric brick solid element has been implemented.

Lewis Contact: C. Lawrence (216) 433-6048

ANALYSIS OF CASCADES USING A TWO-DIMENSIONAL EULER AEROELASTIC SOLVER

Flutter is a self excited vibration which leads to blade failure in propfans, compressors and turbines. A fair understanding of the flutter phenomenon can be obtained by analyzing a two dimensional version of the propfan, compressor or turbine. This two dimensional version is called a cascade. In the present effort, an aeroelastic solver was developed to investigate the flutter behavior of two-dimensional oscillating cascades. The required unsteady aerodynamic forces were obtained from solving the two-dimensional, unsteady Euler equations. The cascades can have subsonic, transonic, or supersonic flow with either subsonic or supersonic axial velocity. The Euler equations were solved by using a flux differencing scheme. The solution scheme is third-order accurate in space and second-order accurate in time. The flow equations were solved on one or more passage-centered H-grids. The aerodynamic solver was coupled with a typical section structural model for each blade of the cascade. The typical section had two degrees of freedom (bending and torsion) for each blade. Flutter analysis methods both in time and frequency domains were implemented into the resulting aeroelastic solver. The flutter stability was assessed from an eigen analysis in the frequency domain. In the time-domain method the aeroelastic equations were integrated simultaneously in time to calculate the aeroelastic response. The response indicated the stability. Methods that reduce computational time for calculating the unsteady aerodynamic coefficients, namely the influence coefficient (IC) method and the pulse response (PR) method, were also implemented and validated. The present solver showed good correlation with published results for all the flow regimes. A representative flutter calculation showed that both the frequency-domain and the time-domain methods were implemented correctly into the aeroelastic solver. Some typical results are shown in figures 1 and 2.

Figure 1 shows the predicted distribution of the unsteady pressure difference coefficient when the blades of the cascade are vibrating with a phase angle (σ) of 90° between them; results from the linear theory are also plotted for comparison. The cascade parameters are a gap-to-chord ratio s/c of 1.538 and a stagger angle (Θ) of 45°. The flow parameters are an inlet Mach number (M_∞) of 0.8 and an incidence angle (i) of 0°. The cascade is harmonically oscillated (HO) in pitch about the midchord. The reduced frequency based on the semichord (k_b) is 0.32, and the amplitude of oscillation (α_0) is 0.3°. The results are in excellent agreement with linear theory.

For flutter calculation a tuned cascade with five blades was considered. The parameters were s/c = 1.85, Θ = 10.7 deg., M_∞ = 0.7, and i = 2.15°. The airfoils section was from a NACA 16 series with a thickness-to-chord ratio of 0.03 and a design lift coefficient of 0.3. The structural model for each blade was a typical section (pitching and plunging) with the elastic axis at the leading edge. The mass ratio was 115, the radius of gyration was 1.076, and the offset between the elastic axis and the center of mass was 0.964 semichords; the ratio of natural frequencies in bending and torsion was 0.567. First, a frequency-domain solution was obtained. For the present example the phase angle at flutter was σ = 288°, the ratio of the flutter frequency to torsional frequency = 0.67, and the reduced frequency was k_b = 0.111. These results were in good agreement with the values predicted by a full potential solver. Next, a time-domain response solution was obtained for the same example. Owing to time constraints, calculations have been performed only for the velocity parameter V* = 2.0. One of the blades (here after noted as reference blade) in the cascade was given a small initial pitching velocity. All the other blade displacements and velocities were initially zero. Figure 2 shows the variation of the plunging displacement for the reference blade with time. The pitching displacement for the reference blade, which is not presented here, showed a very similar variation. The plunging and pitching displacements of the remaining four blades, which are not presented here, differed only in their phase of motion with respect to the first blade. The responses showed that the blade motion was decaying, implying that the cascade was stable at V* = 2.0. This value of reduced velocity corresponds to a reduced frequency of k_b = 0.25, which showed positive damping (stable oscillations) in the frequency-domain flutter analysis. This typical solution indicates that the time-domain method shows the aeroelastic behavior as predicted by the frequency-domain method.

Lewis Contact: T.S.R. Reddy (216) 433-6083

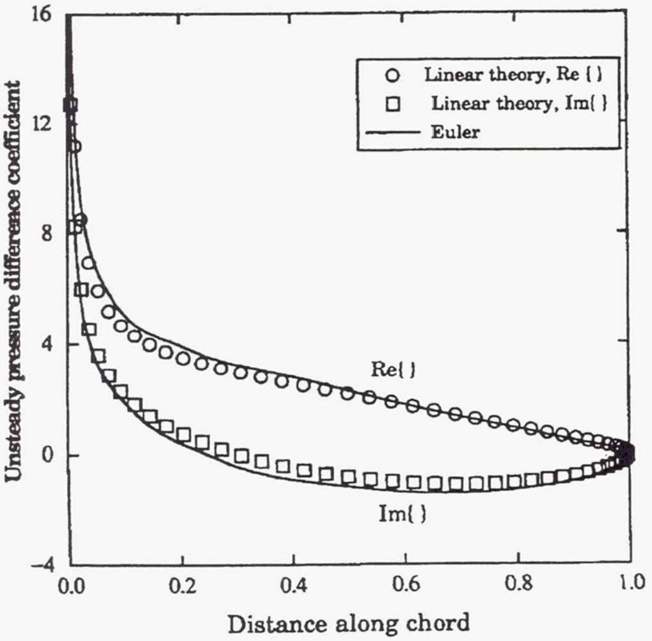

Figure 1. - Flat-plate cascade with pitching about midchord: s/c = 1.538, θ = 45°, M_∞ = 0.8, i = 0°, k_b = 0.32, α_0 = 0.3°, σ = 90°.

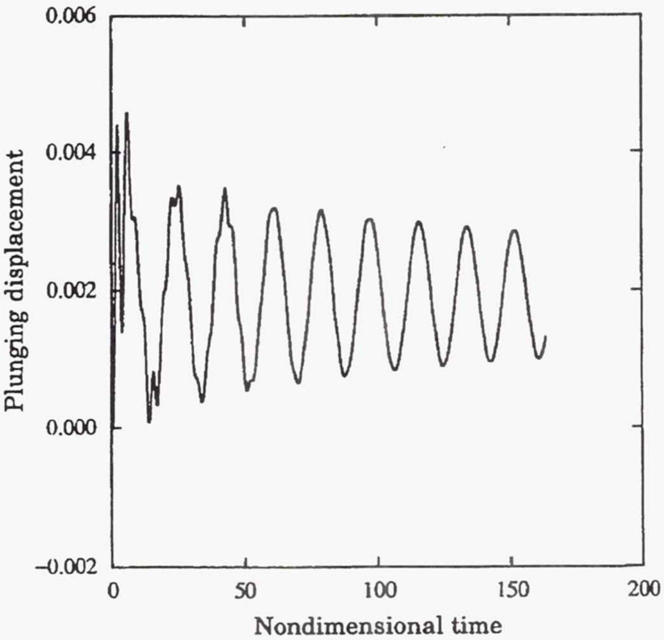

Figure 2. - Plunging displacement of reference blade in two-degree-of-freedom flutter example for reduced velocity V = 2.0.*

EFFICIENT FLUTTER ANALYSIS FOR CAMBERED COMPRESSOR AND TURBINE BLADES

Designers of turbomachinery for aircraft and propulsion systems rely heavily upon simplified flutter analysis methods. These methods are most commonly based upon simple, unsteady aerodynamic theories that disregard the effect of real airfoil shape and off-design flow conditions. A considerable data base of empirical correlations has been compiled to adjust designs so as to achieve aeroelastic stability. The primary motive for using these empirical design systems is that they are cost effective (in computer resources and time) and fairly accurate for design analysis.

Research at NASA Lewis has been devoted to developing advanced unsteady aerodynamic and aeroelastic models that will specifically address the flutter problem. One of the tools that has been developed for NASA Lewis is a linearized, unsteady aerodynamic code (LINFLO) for calculating two-dimensional flows due to airfoil oscillation and wake passing in turbomachinery cascades. This code has been developed under contract to NASA Lewis by United Technologies Research Center. The code applies to airfoils that have large thickness and high camber and flow turning and that operate within subsonic to transonic flow regimes. A distinct advantage of LINFLO is that it assumes harmonic airfoil oscillations, so that the unsteady solution is performed in the frequency domain. Subsonic flutter inception has been found experimentally to be fully linear and to occur at a discrete single frequency. The frequency-domain approach results in several orders of magnitude less computational time than comparable computational fluid dynamics time-domain methods.

A flutter prediction code has been developed that uses LINFLO to compute the unsteady aerodynamic loads. The aeroelastic code is based on a classical two-degree-of-freedom, lumped-parameter structural model of the blade that represents a "typical section" of a full three-dimensional blade. An iterative flutter search technique based on Newton's method is used to pinpoint the conditions under which a flutter instability may occur.

The method has been demonstrated by analyzing a compressor cascade operating under subsonic flows. The compressor blade was modeled as a flat plate, and an NACA 0006 thickness distribution was applied over circular-arc mean camber lines of various camber levels. In addition, a single airfoil case was analyzed over a range of Mach numbers and steady flow incidence angles.

The results from this analysis (see fig. 1) indicate that increasing the airfoil camber stabilized the rotor when considering classical bending-torsion flutter. These results also demonstrate the sensitivity and susceptibility of a cascade to airfoil shape, and in particular the airfoil camber. The same sensitivity has been shown for variations in the inlet flow incidence angle into the cascade. Neglecting the effect of steady aerodynamic loading due to either airfoil shape (thickness and camber) or steady flow incidence can lead to misleading estimates of turbomachinery flutter behavior.

Researcher: T. E. Smith (Sverdrup Technology)

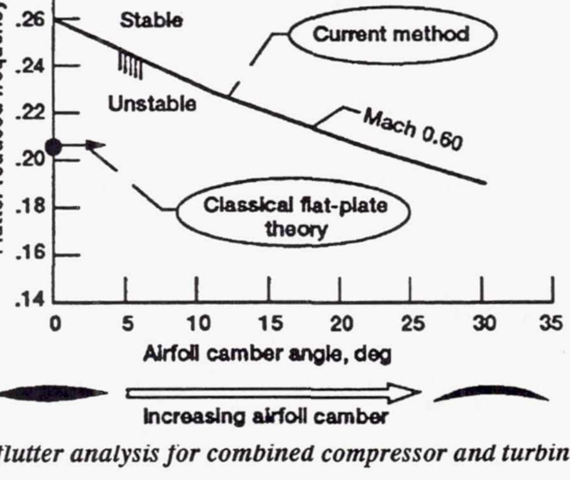

Results of flutter analysis for combined compressor and turbine blades.

AEROELASTIC STABILITY CHARACTERISTICS OF THE SSME HPOTP TURBINE ROTOR

A dynamic analysis of the first-stage turbine blade for the Space Shuttle Main Engine (SSME) High Pressure Oxidizer Turbopump (HPOTP) was performed wherein the unsteady aerodynamic effect on rotor stability was assessed. The method employed applies modal dynamic analysis to simulate the coupled blade/fluid system. A three-dimensional finite element model of the blade was used in conjunction with two-dimensional linearized unsteady aerodynamic theory. The aerodynamics were modeled by placing axisymmetric stream-surface strips along the blade span. The blade structural and aerodynamic behaviors were coupled within modal space. A complex eigenvalue problem was solved to determine the stability of the tuned rotor system.

The aeroelastic analysis was applied to the SSME HPOTP first-stage turbine operating at 109% rated power level. This blade was modeled by using six axisymmetric stream surfaces along the airfoil span and by retaining the first four normal modes of the turbine blade. The aeroelastic computations using these modes found that the aerodynamic damping levels were low (less than 0.5% of critical damping) for all modes of vibration. The second normal mode (edgewise mode) was found to be unstable for interblade phase angles from 18° to 22Γ . The root loci of all calculated eigenvalues for motion in the first and second modes are shown in the figure. This analysis did not consider the effects of mechanical and material damping on the blade stability. Damping will generally have a stabilizing effect on the blade.

Blade cracking has been a continuing problem during the development of the HPOTP, although not as acute a problem since the introduction of blade-to-blade friction dampers at the blade platforms. The results from this analysis indicate that the history of blade cracking may be due to an unstable limit cycle vibration in the edgewise mode caused by flutter instability.

Lewis Contact: D. Murthy (216) 433-6714

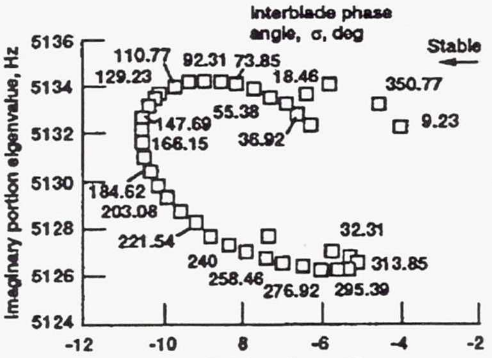

(a) First bending motion.

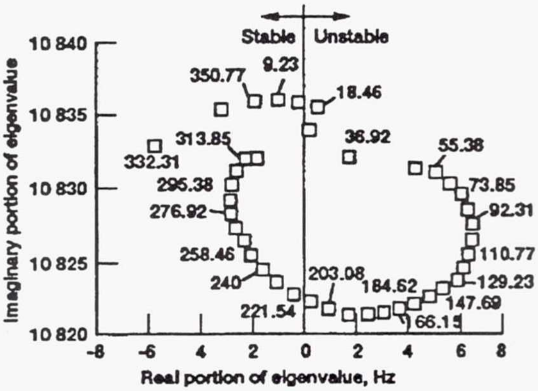

(b) First edgewise motion.

Plot of root locus for turned HPOTP turbine vibration.

UNSTEADY AERODYNAMIC ANALYSES FOR TURBOMACHINERY FLUTTER AND FORCED RESPONSE

The objective of this research program is to develop theoretical, unsteady aerodynamic models and computer codes for predicting compressible, unsteady, inviscid and viscous flows through the blade rows of axial-flow turbomachines. Such analyses are needed to understand the effect of unsteady aerodynamic phenomena on the structural stability, noise generation, and aerodynamic performance of the blading. They will apply to the prediction of flutter, forced vibration, and the aeroacoustic response of turbomachinery fan, compressor, and turbine blading operating at subsonic and transonic Mach numbers.

Emphasis is being placed on developing theoretical analyses that are based on asymptotic representations of unsteady flow phenomena. Thus, flows that are driven by small-amplitude unsteady excitations in which viscous effects are concentrated in thin layers are being considered. The resulting analyses will apply in most practical situations, will lead to a strong fundamental understanding of the important physical phenomena, and will be computationally efficient. Therefore, they will be appropriate for implementation into turbomachinery aeroelastic and aeroacoustic design prediction systems.

The unsteady aerodynamic behavior of turbomachinery blading is strongly dependent on the underlying steady background flow. Because of loading effects and blade geometry, blade rows operate in nonuniform, steady flow environments. The linearized inviscid unsteady aerodynamic analysis, LINFLO, models small unsteady disturbances caused by prescribed blade motions and/or external aerodynamic disturbances which carry energy toward the blade row as first-order or linear perturbations of the mean flow variables.

Under this research program the LINFLO analysis has been extended to predict the unsteady blade loads that are excited by entropic and vortical "gusts." Also, an unsteady viscous-layer analysis and code (UNSVIS) has been extended and coupled to the linearized inviscid analysis to provide a weak viscid/inviscid interaction solution capability for unsteady cascade flows. At present a more accurate inviscid steady flow analysis (SFLOW) is being developed to be used in conjunction with LINFLO, and a simultaneous coupling of nonlinear inviscid and viscous-layer analyses is being developed to provide a strong inviscid/viscid interaction capability (SFLOW-IVI) for steady cascade flows. In the future a strong inviscid/viscid interaction analysis will be developed for unsteady cascade flows.

Special consideration must be given to flows in which the unsteady perturbation is due to an entropic or vortical excita-

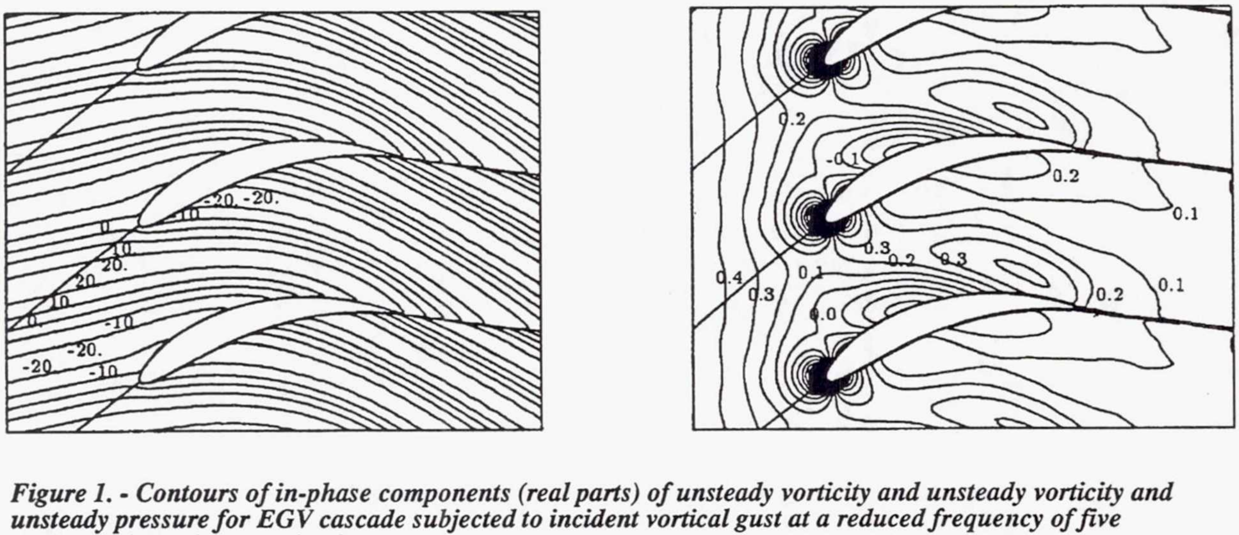

Figure 1. - Contours of in-phase components (real parts) of unsteady vorticity and unsteady vorticity and unsteady pressure for EGV cascade subjected to incident vortical gust at a reduced frequency of five and interblade phase angle of -2π.

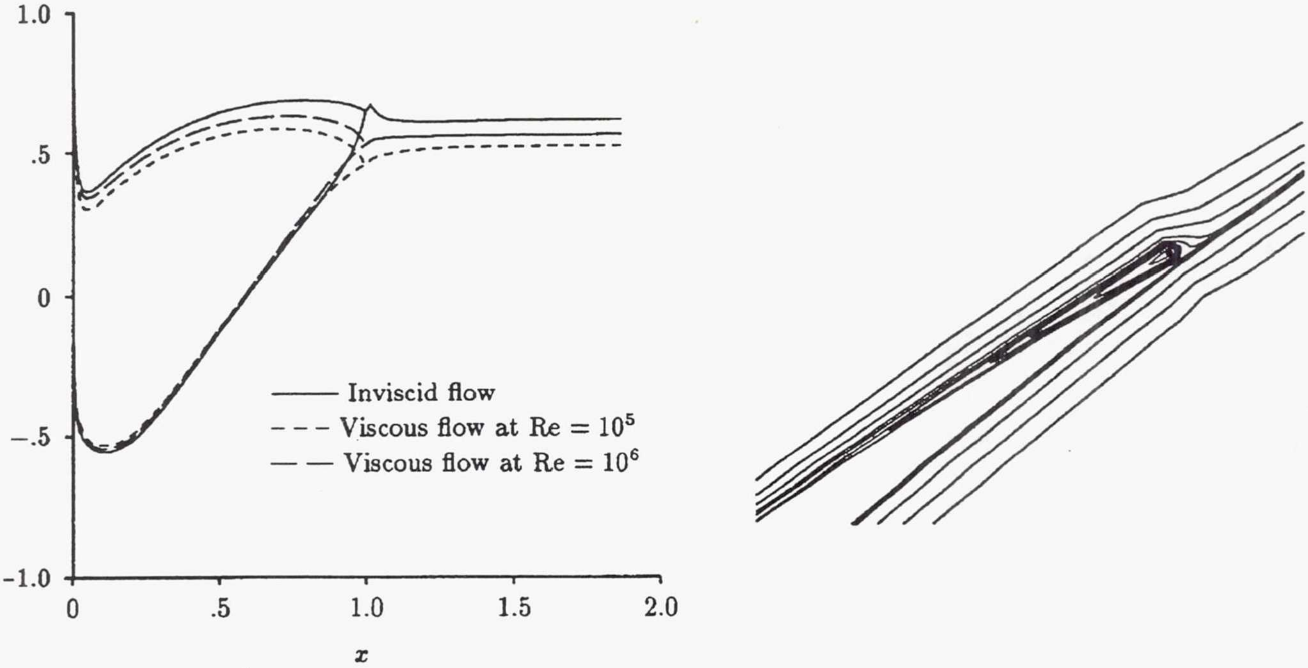

(a) Pressure coefficient vs χ.

(b) Trailing edge streamlines for Re = 10^5.

Figure 2. - Subsonic flow through a high-speed compressor cascade.

tion. For subsonic or transonic flows containing weak shocks the steady background flow can be regarded as irrotational and isentropic. In this case the linearized unsteady equations can be greatly simplified by using a velocity-splitting technique due to Goldstein. A distinct advantage of this formulation is that the unsteady flow can be resolved accurately and with minimal computational effort. Figure 1 highlights an application to a compressor exit guide vane (EGV) that is excited by a harmonic vortical (wake) excitation at the inlet. The calculated vorticity field and the unsteady pressure response resulting from the interaction of the vortical gust with the EGV blade row are shown in this figure. The unsteady pressures acting at the blades surface cause blade vibrations that can eventually lead to high-cycle fatigue failures; those acting upstream and downstream of the blade row can eventually lead to discrete-tone noise. The unsteady calculation depicted in figure 1 required less than 10 CPU seconds on a CRAY YMP.

A comprehensive model for predicting unsteady flows in turbomachinery blade passages must account for viscous effects. Thus, steady and unsteady inviscid/viscid interaction (IVI) analyses are also being developed as part of this research effort. At this point a steady analysis has been developed that will provide the foundation for an unsteady analysis to be constructed in the future. The steady IVI analysis couples the nonlinear potential-flow analysis SFLOW with a finite-difference, viscous-layer analysis. The resulting analysis, SFLOW-IVI, is capable of predicting flows in which small-to-moderate viscous-layer separations occur. Numerical results for a high-speed compressor cascade are shown in figure 2, where the pressure coefficient distributions, $C_p(x)$, along the blade and wake are presented for an inviscid flow and for viscous flows at Reynolds numbers (Re) of 10^5 and 10^6. The viscous flow at Re = 10^5 separates from each blade suction surface in the vicinity of the trailing edge, with the separation bubbles extending over 20 percent of blade chord.

Because of the large number of controlling parameters involved, an efficient capability for predicting blade-row unsteady aerodynamic responses to structural and external aerodynamic excitations is a crucial prerequisite for improving aeroelastic and aeroacoustic designs. The analytical research being conducted under this research program is contributing toward meeting this need.

Lewis Contact: D. Murthy (216) 433-6714

DEMONSTRATION OF AEROELASTIC VIBRATION OF ROGUE BLADES IN TURBOMACHNERY

Turbomachinery rotors consist of several nominally identical blades assembled on a disk. These blades operate in an inherently unsteady environment in which the aerodynamic forces interact with the elastic and inertial forces in the blade to produce complex dynamic response. An aeroelastic analysis is required to characterize this interaction.

In real turbomachinery rotors all the blades are not identical. Cyclic symmetry is always disrupted by differences in the blade structural properties, which result from manufacturing and material tolerances. This phenomenon is known as mistuning.

Mistuning tremendously increases the size and cost of the aeroelastic analysis of blade assemblies such as engines and fans. The assumption of identical blades is frequently made, because it yields drastic reductions in computational cost. This assumption allows the equations of motion to be uncoupled, thereby reducing the problem size to that of only one blade. In the aeroelastic response of such an idealized rotor, the vibration energy is equally distributed among all the blades. However, the response of a real rotor may be qualitatively different, leading to unanticipated blade failures. In particular, small random mistuning can drastically alter both the free and the forced aeroelastic response by localizing the vibration energy to a few rogue blades, leading to very high stresses in these blades. This phenomenon is known as mode localization.

We have demonstrated analytically that mode localization can occur in realistic turbomachinery rotors because of aerodynamic coupling. A rotor having blades with random mistuning in their natural frequencies was examined. Each blade was modeled as a straight, slender, twisted, nonuniform elastic beam with a symmetric cross section, that is clamped rigidly to the disk. The equations of motion of a rotating blade were discretized by a standard assumed-mode procedure. Root and disk flexibility were neglected to keep the focus on the aerodynamic coupling in the rotor. The unsteady aerodynamic forces were calculated by using two-dimensional, linear, unsteady, cascade aerodynamic theories in a strip fashion for both subsonic and supersonic regimes.

The rotor examined in this study is representative of a forward stage of an advanced axial-flow compressor. Only one component blade mode, the first torsion mode, was considered.

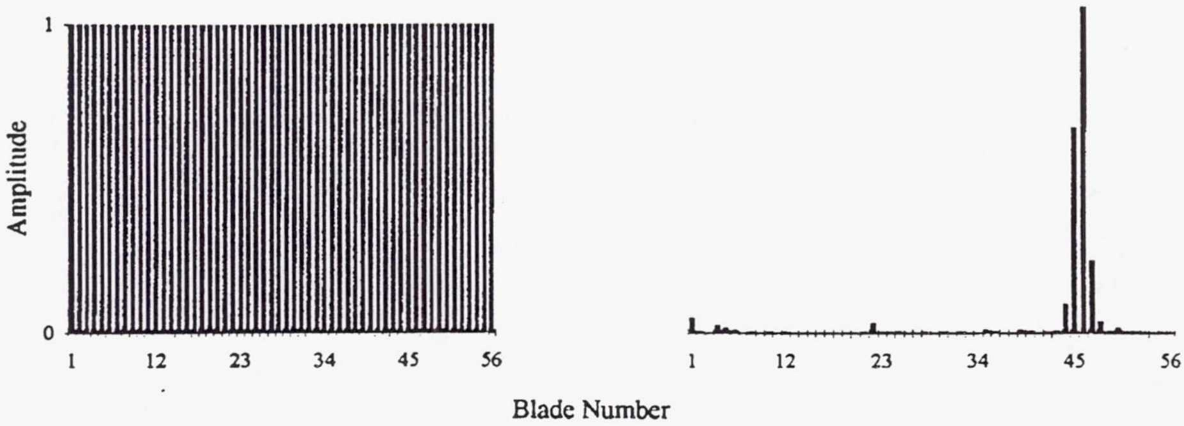

(a) Tuned

(b) 4.67% Mistuned

Figure 1. - Aeroelastic mode shape associated with lowest frequency eigenvalue for tuned and mistuned cases. Note the confinement of vibration to a few blades.

When mode localization occurs, the aeroelastic mode shapes are fundamentally altered. As shown in figure 1, the vibration was confined to a small number of blades that absorbed all the energy of excitation. The constant interblade-phase-angle behavior of the idealized system was lost. Moreover, the regular structure that is characteristic of the root locus of the tuned system, became randomly scattered (see fig. 2). Localization became more severe as the level of mistuning increased. At any given level of mistuning, the lowest and highest frequency modes were the first to localize and had the most severe localization. The degree of localization increased with the number of blades on the rotor.

It was found that the strength of aerodynamic coupling played a critical role in the aeroelastic mode localization phenomenon. The nature of aerodynamic coupling in typical turbomachinery rotors is such that aerodynamic interblade coupling is weak in the sense that the unsteady aerodynamic forces are very small in magnitude relative to the elastic and inertia forces. The weak nature of the aerodynamic coupling makes turbomachinery rotors susceptible to aeroelastic mode localization and rogue blade behavior for even small levels of mistuning that cannot be avoided in practice.

Lewis Contact: D. Murthy (216) 433-6714

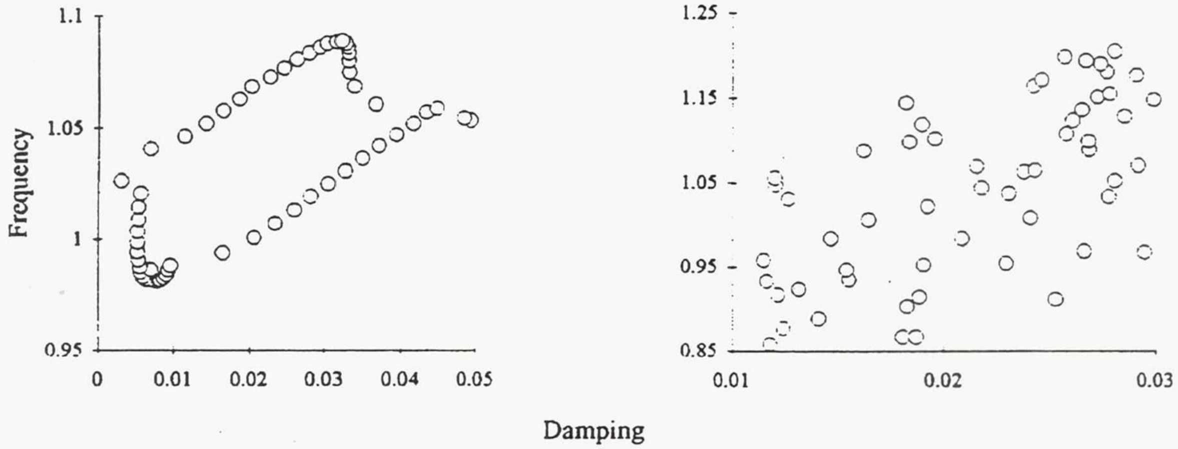

(a) Tuned

(b) 4.67% Mistuned

Figure 2. - Root locus of aeroelastic eigenvalues in complex plane. Note the scattering of the root locus with moderate mistuning.

PERTURBATION METHODS ENABLE RAPID TRADE-OFF STUDIES TO AVOID ROGUE BLADE BEHAVIOR IN TURBOMACHINERY

In real turbomachinery rotors all the blades are not identical. Cyclic symmetry is always disrupted by differences in the blade structural properties, which result from manufacturing and material tolerances. This phenomenon is known as mistuning.

Mistuning tremendously increases the size and cost of the aeroelastic analysis of blade assemblies such as engines and fans. The assumption of identical blades is frequently made because it yields drastic reductions in computational cost. This assumption allows the equations of motion to be uncoupled, thereby reducing the problem size to that of only one blade. In the aeroelastic response of such an idealized rotor the vibration energy is equally distributed among all the blades. However, the response of a real rotor may be <u>qualitatively</u> different, leading to unanticipated blade failures. In particular, small random mistuning can drastically alter both the free and the forced aeroelastic response by <u>localizing</u> the vibration energy to a few rogue blades leading to very high stresses in these blades. This phenomenon, known as mode localization, has been previously demonstrated in the presence of structural as well as aerodynamic coupling in realistic turbomachinery models.

Perturbation schemes that predict and provide insight into mistuning effects and mode localization phenomenon were developed. First, a standard, or classical perturbation scheme that predicts high sensitivity to mistuning was applied. Then, a perturbation scheme that is able to handle relatively large mistuning effects and thus to characterize the localized modes of vibration, was developed. The latter is referred to as "the modified perturbation scheme".

In the classical scheme, the unperturbed system was the tuned assembly and the perturbation was the frequency mistuning. First order classical perturbation analysis for eigenvalues showed that there is no first-order effect of mistuning on the flutter boundary (fig. 1). Also, to first order, all the system eigenvalues are shifted identically as a result of mistuning, by an amount equal to the average of the deviations of the frequencies squared from the nominal value. For small mistuning the eigenvalue shift is always small. The first-order classical perturbation analysis for eigenvectors provides a rich set of insights. For example, it reveals that the aeroelastic mode shapes are highly sensitive to mistuning when the ratio of mistuning to interblade coupling is of first order. This was verified to be true by exact calculations. Also, the sensitivity to mistuning, or equivalently the tendency to vibration localization, increases with the number of blades. The specific interactions among mistuning, aerodynamic coupling, and number of blades that affect the vibration localization phenomenon are apparent from the expressions.

The second-order classical perturbation expressions for eigenvalues show much the same trends as the first-order classical perturbation expressions for eigenvectors, but in a more compact form. In particular, these expressions confirm that, when mistuning is introduced, the system root locus expands in the frequency direction and shrinks in the damping direction. This explains the well-known stabilizing effect of mistuning in flutter analysis. The classical perturbation methods fail to describe the dynamics of a mistuned assembly when it is qualitatively different from that of the corresponding tuned system (fig. 1). Nevertheless, they predict high sensitivity and provide useful insights into the onset of mode localization.

The main motivation behind the development of the modified perturbation scheme was that high sensitivity is caused by the small interblade coupling and hence this small parameter must be treated as a perturbation. The mistuning was included in the unperturbed state. The unsteady aerodynamic forces provided the perturbation. Thus, the modified perturbation analysis is valid for large mistuning (fig. 2) or relatively small aerodynamic coupling. This is precisely the range for which the classical perturbation analysis breaks down. The first-order modified perturbation analysis provides expressions for localized mode shapes. The mechanism of localization is clarified by these expressions. For example, the vibration amplitude of a blade is directly proportional to the amount of aerodynamic coupling between that blade and the large amplitude blade (rogue blade) and inversely proportional to the difference between its stiffness and that of the rogue blade. Also, the location of the rogue blade is revealed in terms of the blade stiffnesses and the aerodynamic coupling among them.

In summary, the perturbation expressions developed in this work provided several qualitative insights into the aeroelastic vibration characteristics of mistuned turbomachinery blade assemblies and enabled prediction of rogue blade location on the rotor.

Researchers: D. V. Murthy (University of Toledo) and C. Pierre (University of Michigan)

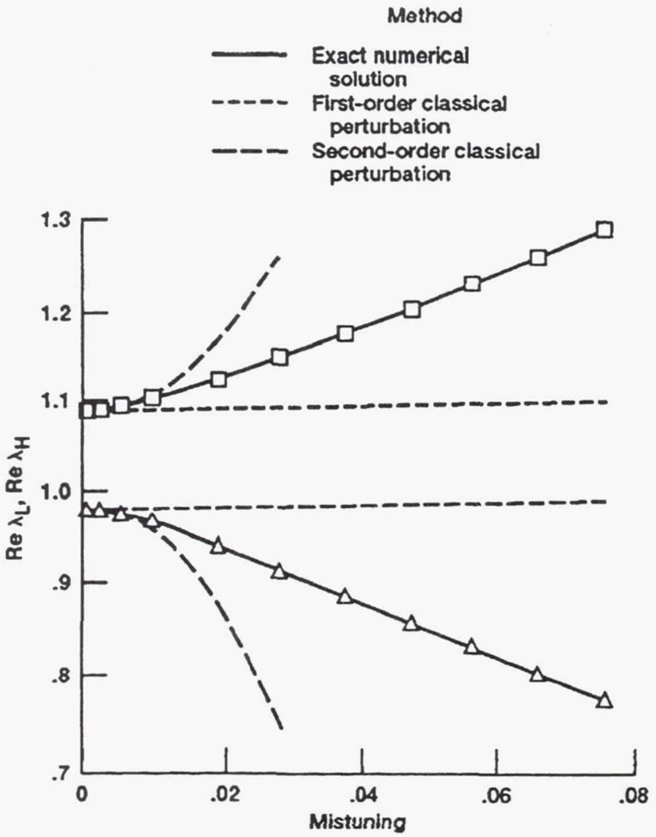

Figure 1.

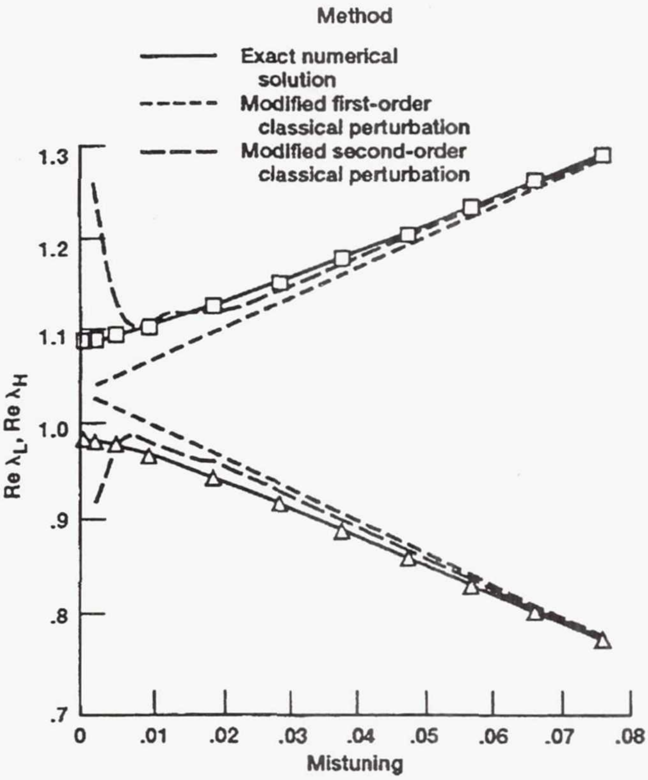

Figure 2.

Loci of real parts (frequency) of lowest and highest frequency eigenvalues versus mistuning by "exact" numerical solution and modified perturbation methods.

SUBSONIC/TRANSONIC CASCADE FLUTTER USING A FULL-POTENTIAL SOLVER

A time-accurate, two-dimensional, full-potential solver was applied to flutter calculations in subsonic/transonic flow. The unsteady aerodynamic coefficients required in a frequency-domain flutter analysis were calculated efficiently by linear methods. The influence coefficient method and the pulse response method were used to generate the aerodynamic lift and moment coefficients for different interblade phase angles and different oscillation frequencies, respectively. The combined pulse response and influence coefficient method was used to calculate the aerodynamic coefficients at different combinations of oscillation frequency and interblade phase angle. All the calculations were verified by comparison with results from the harmonic oscillation method and with other published results. Excellent correlation was seen in all cases even when shocks were present in the flow field.

Frequency-domain and time-domain flutter calculations were performed for a cascade of NACA 64A010 airfoils (see figure); both approaches yielded comparable results because only small amplitudes of motion were considered. Prominent differences were seen between the cascade results at different phase angles. These results for the most unstable phase angle were qualitatively similar to published results for isolated airfoils. The most important difference was that the flutter speed and flutter frequency for the cascade reach a minimum at a lower Mach number.

Lewis Contact: M. A. Bakhle (216) 433-6037

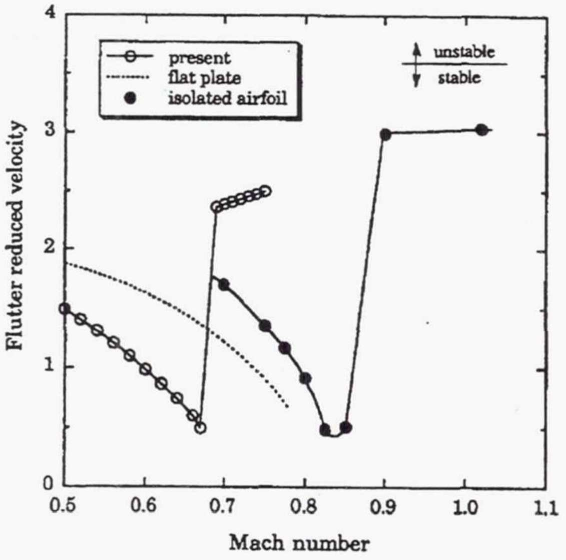

Flutter velocity for NACA 64A010 cascade at interblade phase angle of 45°.

OPTICAL MEASUREMENT OF UNDUCTED FAN FLUTTER

Flutter blade vibrations at the near-tip span were successfully measured and monitored during a wind tunnel test of an Unducted Fan model by an optical method. The method relies upon the chopping of the laser beam by the blades rather than upon the reflection of a light beam by the blade tips. The traveling-wave nodal diameter modes were determined from the overall displacement spectra given the frequency, which was measured by strain gages. Because of the presence of mistuning, and because of the incomplete strain gage coverage of the rotor blades, this information could not be obtained from the strain gage data alone.

Two distinct flutter modes were present. One was associated with the first natural mode and the other with the second. An indication of a flutter mode shape was obtained from the displacement data as the ratio of the leading- to trailing-edge flutter amplitudes (fig.). For each mode this ratio was in the neighborhood of the corresponding calculated value obtained from a finite element code that accounted only for centrifugal loads. For both modes, however, the experimentally determined amplitude ratios were lower and frequencies were somewhat higher than the calculated values. The frequency spread for the first flutter mode for the range of nodal diameters encountered in the test was relatively small; however, it was rather large for the second flutter mode, particularly for the -2-nodal-diameter group, which also occurred at a high relative Mach number. For this traveling-wave mode, most flutter points occurred close to the 4 E frequency. Past a certain flutter amplitude level, rapid spontaneous amplitude growth was observed for these points. In addition to the well-defined flutter frequency peak, the amplitude growth was also evident in a frequency band of about 0.2 E on either side of 4 E. The 4 E forced response was evident in the strain gage spectra away from the flutter region. Its source is unknown. For the high tip relative Mach numbers, spontaneous growth was also observed for the -1-nodal-diameter group. The second-flutter-mode points corresponding to the zero nodal diameter occurred at the lower relative Mach numbers and were all close to the second natural frequency.

Some evidence of secondary response at nonintegral engine orders was noticed and associated with the positive interblade phase angles at frequencies that were, in general, close to the second natural mode but with a much higher leading- to trailing-edge amplitude ratio. This ratio was essential in sorting out these points.

For both flutter modes, high incidence was found to be destabilizing.

Researcher: A. P. Kurkov (NASA Lewis)

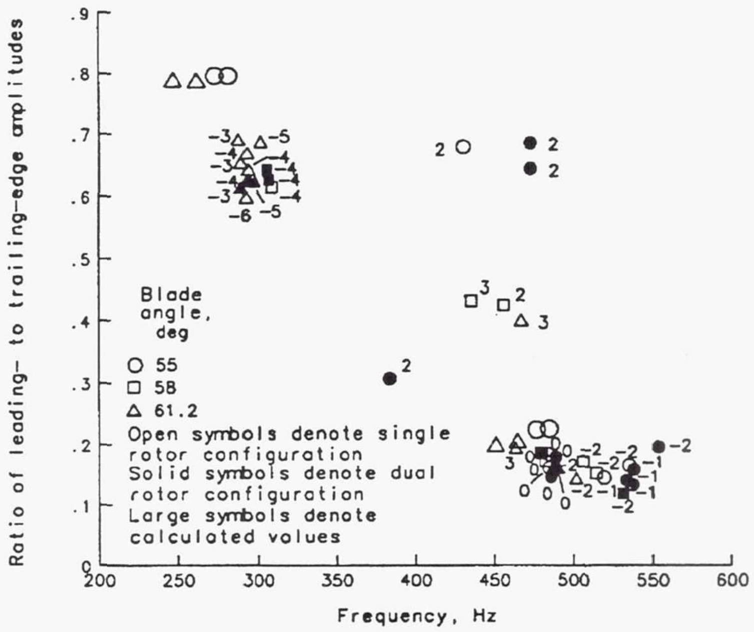

Ratio of leading to trailing-edge flutter amplitude and modal diameters.

EFFICIENT COMPUTATION OF AERODYNAMIC INFLUENCE COEFFICIENTS FOR AEROELASTIC ANALYSIS ON A TRANSPUTER NETWORK

Aeroelastic analysis is multidisciplinary and computationally expensive. Hence, it can greatly benefit from parallel processing. As a part of an effort to develop an aeroelastic analysis capability on a distributed-memory multiple processor computer, a parallel algorthim for the computation ofaerodynamic influence coefficients was implemented on a network of 32 transputers. The network is connected to a root transputer that is hosted by a IBM/AT-compatible personal computer. A transputer is a microprocessor on a single chip that is designed by INMOS Corporation specifically for parallel processing.

Within an advanced aeroelastic analysis program called ASTROP3, the aerodynamic influence coefficients are calculated by using a three-dimensional unsteady aerodynamic model and a panel discretization. On the Cray XMP supercomputer the computation of the influence coefficients uses 97 percent of the total execution time for a representative case with a model of the SR3C-X2 propfan blade. Fortunately, this computation has a high degree of independence and thus can be done concurrently on separate processors.

To achieve efficient computation on a parallel processing network, the computational load must be balanced among all the processors. This is difficult when each subtask requires differing amounts of execution time. For the transputer network, the order of subtask execution had a significant effect on the computational speedup for a representative propfan blade case. As shown in figure 1, a "diagonal" execution order, in which the longest subtasks were started first, improved speedup to 26.7 from 20.5 for a standard execution order with 32 processors.

Improved computational speedup also resulted from changes in network topology. A binary tree network gave slightly higher speedup ratios than a simple pipeline network. This result was due to the smaller number of communication steps in the binary tree network.

The distributed-memory transputer system had significantly better speedup results than the shared memory Alliant FX/80 computer. As shown in figure 2, the transputer network achieved a speedup of 7.7 for eight processors versus 6.2 for an eight processor FX/80. However the FX/80 was much faster because of its sophisticated vector processors.

Lewis Contact: D. C. Janetzke (216) 433-6041

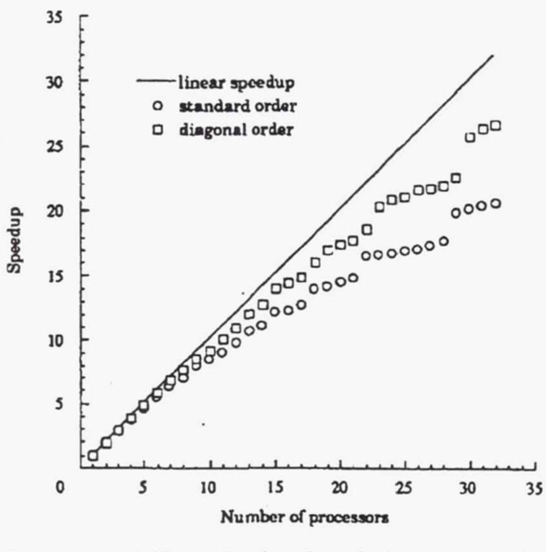

Figure 1. - Effect of subtask ordering on speedup.

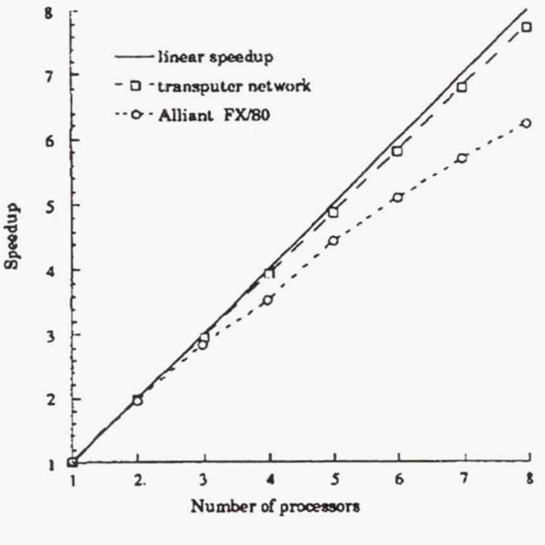

Figure 2. - Speedup comparison between distributed- and shared-memory architecture computers.

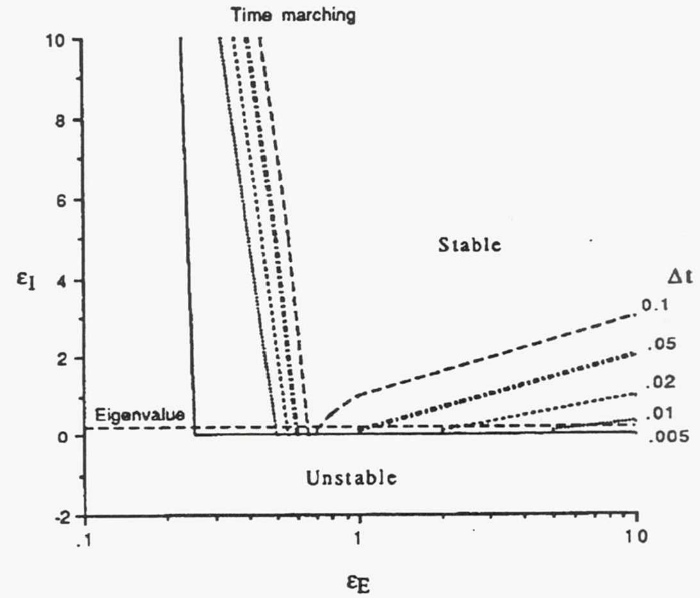

Figure 1. - Stability boundary as function of ε_E, ε_I for different time stepsizes.

ROLE OF ARTIFICIAL VISCOSITY IN EULER AND NAVIER-STOKES SOLVERS

Considerable research has been conducted during the last few years to develop methods for solving the Navier-Stokes equations. Finite difference schemes or finite element techniques are used to solve these equations. These methods involve a numerical description of the governing equations, a finite number of grid points or elements in the flow field, and a linear or iterative treatment of nonlinear terms. These solution algorithms usually have stability problems when a computation is initiated with approximate starting data or when the finite spatial discretization is unable to resolve large gradients in flow variables. The stability analysis of the solution algorithms for the Navier-Stokes equations is usually done by applying these algorithms to the wave equation or the heat equation and studying their stability. Then these algorithms are implemented for the Navier-Stokes equations, and artificial viscosity terms in various forms are added so as to obtain stable solutions for many different flow cases. These artificial viscosity terms are often modified to allow for shock resolution, finite spatial discretization, and experimental verification. Note that artificial viscosity tends to reduce all gradients in the solution whether physically correct or numerically induced. When time-marching codes based on the Navier-Stokes equations are used to study physical instabilities such as flutter, it is important to first understand the influence of artificial viscosity on numerical instabilities.

An eigenvalue stability analysis was applied to a Navier-Stokes solver for flow over airfoils. The effect of artificial viscosity terms was studied to determine how time marching the solution affects stability and also the effect on stability as indicated by the eigenvalue calculation. The stability and growth of small perturbations about a steady flow over airfoils were analyzed for various amounts of artificial viscosity. The eigenvalues were determined for a small time-dependent perturbation about a steady inviscid flow over an NACA 0012 airfoil at a Mach number of 0.8 and angle of attack of 0°.

The method has been applied to inviscid flows here but as discussed is also applicable to viscous flows. The stability boundaries as a function of the amount of artificial viscosity ($\in_E$ controls the amount of explicit artificial viscosity and $\in_I$ controls the amount of implicit smoothing) from both the eigenvalue analysis and the time-marching scheme are shown in figure 1. A large number of calculations with many different combinations of $\in_E$ and $\in_I$ were performed to obtain these stability boundaries. In the time-marching code, these boundaries also depended on the time stepsize (Δt) used. The eigenvalue calculation, because of the analytical treatment of time derivatives, corresponded to a time stepsize of zero. A section of the stability boundaries is shown in the Δt, $\in_E$ plane for two different values of $\in_I$ in figure 2. These sections can be extrapolated to $\Delta t = 0$ for a comparison with the eigenvalue stability analysis. It can be seen that, as Δt tends to zero, the amount of artificial dissipation needed for a stable solution also tends to zero. From figures 1 and 2, it can be confirmed that, in the limit as t goes to zero, the stability boundaries from both the eigenvalue and time-marching calculations are in agreement. The eigenvalue procedure not only allows for determining the effect of varying amounts of artificial viscosity, but also allows for the effects of different forms of artificial viscosity. It can also be used to analyze the effects of various other factors, such as the continuous physical problem, the discretization scheme, the physical and numerical boundary conditions, the steady-state flow field, and the grid density and size.

Researchers: A. J. Mahajan (University of Toledo), E. H. Dowell and D. B. Bliss (Duke University), and G. L. Stefko (NASA Lewis)

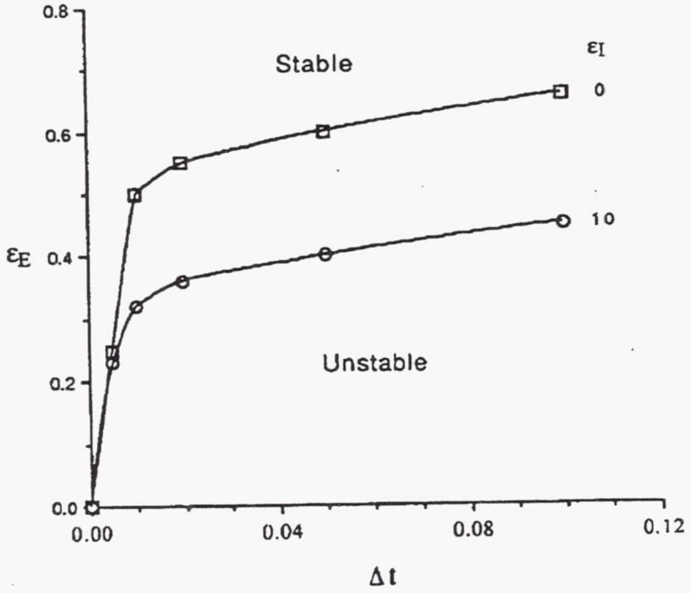

Figure 2. - Stability boundary sections in Δt, ε_E plane for different ε_I.

EIGENVALUE CALCULATION PROCEDURE FOR AN EULER/NAVIER-STOKES SOLVER WITH APPLICATION TO FLOWS OVER AIRFOILS

Eigensystem analysis of dynamic equilibrium equations for a structural system has been a standard procedure among researchers for many years. Dynamic equilibrium equations for a structure are written either in a finite difference or a finite element form. The mass, stiffness, and damping matrices are calculated in order to formulate an eigenvalue problem for the structure. With the advent of larger and faster computers, it is possible to analyze structures of increasing complexity, starting with strings, beams, plates, shells, truss assemblies, etc. Various methods have been developed to determine eigenvalues and corresponding eigenvectors for these structural dynamics equations. The matrices involved in eigensystem calculation are real, symmetric, and sometimes positive definite. Also they can be formed easily once the governing equations are discretized.

In fluid dynamics, nonlinearity in the governing equations and the use of an Eulerian reference frame make it very difficult to formulate an eigensystem analysis. Discretization schemes, block treatment of variables, and linearized solution procedures used in fluid dynamics problems further complicate the formulation of an eigensystem analysis. The existing eigensystem analysis procedures that were developed for structural dynamics problems are thus clearly incapable of modeling fluid dynamics problems.

A Lanczos procedure was developed and applied to a Navier-Stokes solver for computing eigenvalues and eigenvectors. These eigenvalues and eigenvectors are associated with small perturbation analysis of a finite difference repre-

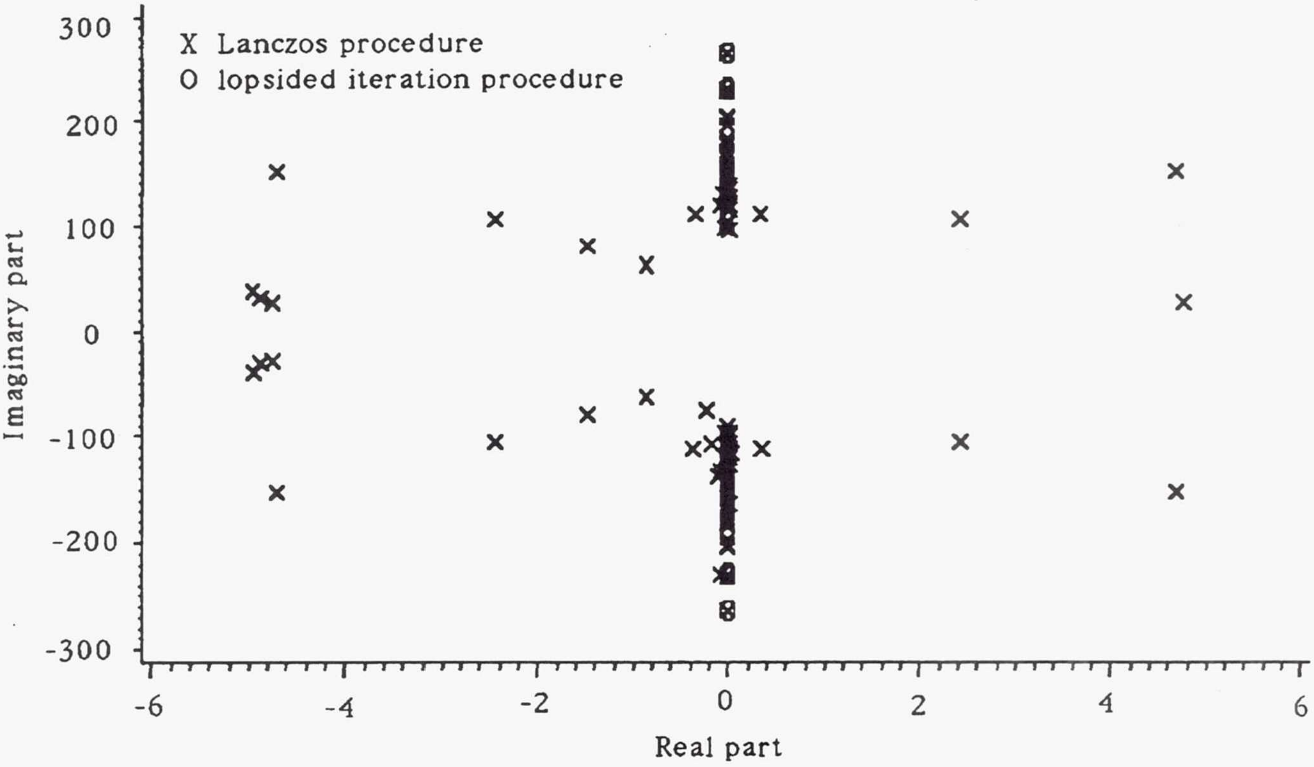

Comparison of "good" eigenvalues from Lanczos procedure with "converged" eigenvalues from lopsided iteration procedure. (NACA 0012 airfoil, inviscid flow, $\alpha = 0°$, $\varepsilon_I = 0$, $\varepsilon_E = 0$.)

sentation of the Navier-Stokes equations for flows over airfoils. A combination of block tridiagonal matrices was converted into a two-dimensional matrix for this eigensystem calculation. This matrix is very large, sparse, real, and nonsymmetric. A separate procedure, which is based on lopsided iteration, was also used to determine the eigensystem. The results from these two procedures are compared in figure 1. The Lanczos procedure provided complete spectral information about the eigenvalues, whereas the lopsided iteration provided only a few of the eigenvalues that were largest in magnitude and the corresponding eigenvectors. The lopsided iteration procedure required much more computer memory and time than the Lanczos procedure. Such eigensystem information is central to transient stability analysis of Navier-Stokes solvers for determining the modal behavior of fluid in a fluid-structure interaction problem and for developing reduced-order models based on variational principles for Navier-Stokes solvers.

Lewis Contact: A. J. Mahajan (216) 433-6034

REPORT DOCUMENTATION PAGE

Form Approved
OMB No. 0704-0188

1. AGENCY USE ONLY (*Leave blank*)	**2. REPORT DATE** December 1992	**3. REPORT TYPE AND DATES COVERED** Technical Memorandum

4. TITLE AND SUBTITLE Structural Dynamics Branch Research and Accomplishments for FY 1992	**5. FUNDING NUMBERS** WU–505–63–513
6. AUTHOR(S) Charles Lawrence	
7. PERFORMING ORGANIZATION NAME(S) AND ADDRESS(ES) National Aeronautics and Space Administration Lewis Research Center Cleveland, Ohio 44135–3191	**8. PERFORMING ORGANIZATION REPORT NUMBER** E–7237
9. SPONSORING/MONITORING AGENCY NAMES(S) AND ADDRESS(ES) National Aeronautics and Space Administration Washington, D.C. 20546–0001	**10. SPONSORING/MONITORING AGENCY REPORT NUMBER** NASA TM–105824

11. SUPPLEMENTARY NOTES

Responsible person, Charles Lawrence, NASA Lewis Research Center, (216) 433–6048.

12a. DISTRIBUTION/AVAILABILITY STATEMENT Unclassified - Unlimited Subject Category 39	**12b. DISTRIBUTION CODE**

13. ABSTRACT ***(Maximum 200 words)***

This publication contains a collection of fiscal year 1992 research highlights from the Structural Dynamics Branch at NASA Lewis Research Center. Highlights from the branch's major work areas—Aeroelasticity, Vibration Control, Dynamic Systems, and Computational Structural Methods are included in the report as well as a listing of the fiscal year 1992 branch publications.

14. SUBJECT TERMS Structural dynamics; Aeroelasticity; Vibration control	**15. NUMBER OF PAGES** 36
	16. PRICE CODE A03

17. SECURITY CLASSIFICATION OF REPORT Unclassified	**18. SECURITY CLASSIFICATION OF THIS PAGE** Unclassified	**19. SECURITY CLASSIFICATION OF ABSTRACT** Unclassified	**20. LIMITATION OF ABSTRAC**